

Aggregation of phosphorescent Pd(II) and Pt(II) complexes with lipophilic counter-anions in non-polar solvents

Ning Zhou,^a Chao Zou,^{*ab} Sa Suo,^{a†} Yuliang Liu,^{a‡} Jinqiang Lin,^a Xiaobao Zhang,^a Minglin Shi,^a Xiaoyong Chang^a and Wei Lu^{*a}

a. Department of Chemistry, Southern University of Science and Technology, Shenzhen, Guangdong 518055, P. R. China. E-mail: luw@sustech.edu.cn.

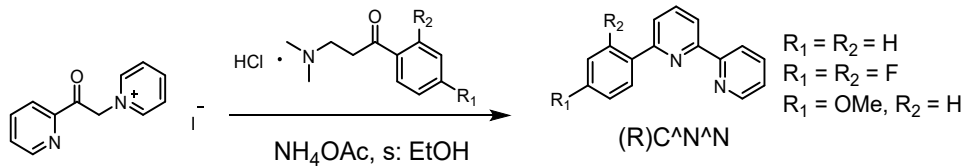
b. Functional Coordination Material Group-Frontier Research Center, Songshan Lake Materials Laboratory, Dongguan, Guangdong 523808, P. R. China.

† Current address: Department of Chemistry, Emory University, Atlanta, 30322, Georgia, USA.

‡ Current address: Division of Chemistry and Biological Chemistry, School of Physical and Mathematical Sciences, Nanyang Technological University, 637371, Singapore.

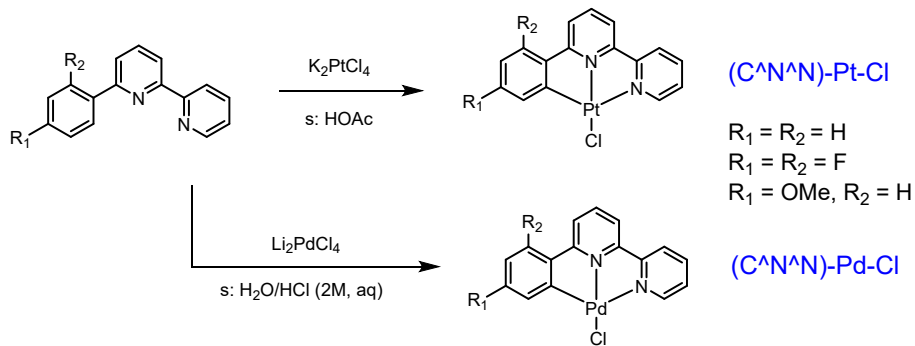
Synthesis and Characterization

Syntheses of C^NN ligands (HC^NN = 6-(2-R₂,4-R₁-phenyl)-2,2'-bipyridine; R₁ = R₂ = H, or F, or R₁ = OMe, R₂ = H) ligands and corresponding [(C^NN)-Pd-Cl] and [(C^NN)-Pt-Cl] complexes



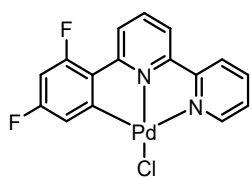
Scheme S1. The synthetic route for the C^NN ligand.

As demonstrated in Scheme S1, C^NN ligand was synthesized according to the modified literature methods.¹ The purities of the ligands were verified by the NMR spectra, comparing with the literature values.



Scheme S2. The synthetic procedure of [(C^NN)-Pt-Cl] and [(C^NN)-Pd-Cl].

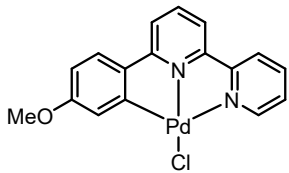
The synthetic procedure of [(C^NN)-Pt-Cl] and [(C^NN)-Pd-Cl] are illustrated in Scheme S2. [(C^NN)-Pt-Cl] was synthesized via literature methods and confirmed by NMR spectra.¹ [(C^NN)-Pd-Cl] was prepared by using corresponding ligands (1 mmol) reacting with Li₂PdCl₄ (1 mmol, 262 mg) in aqueous solution (20 mL) containing 4 mL HCl (2 M, aq), according to the literatures.²⁻³ After 24 h refluxing, the light yellow or yellowish green solid was obtained by filtration, washed with H₂O, MeOH and Et₂O successively, and dried in the air.



Yellowish green solid obtained (370 mg, yield: 90%).

¹H NMR (500 MHz, DMSO-d₆) δ 8.58 (d, *J* = 4.2 Hz, 1H), 8.50 (d, *J* = 8.0 Hz, 1H), 8.28 (dt, *J* =

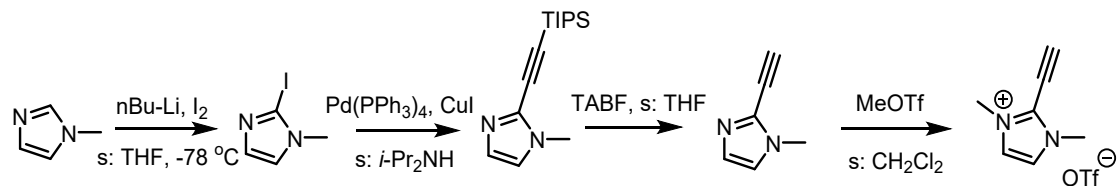
7.8, 3.0 Hz, 2H), 8.19 (t, J = 8.0 Hz, 1H), 7.86 (d, J = 7.9 Hz, 1H), 7.83 – 7.74 (m, 1H), 7.06 (dd, J = 7.9, 2.4 Hz, 1H), 6.97 (s, 1H). ^{19}F NMR (376 MHz, DMSO) δ –105.75 (d, J = 8.9 Hz), –109.76 (d, J = 8.9 Hz).



Yellowish green solid obtained (320 mg, yield: 80%).

^1H NMR (500 MHz, DMSO- d_6) δ 8.65 (d, J = 4.2 Hz, 1H), 8.50 (d, J = 8.0 Hz, 1H), 8.27 (td, J = 7.9, 1.6 Hz, 1H), 8.18 – 8.07 (m, 2H), 7.90 (dd, J = 7.6, 1.1 Hz, 1H), 7.83 – 7.75 (m, 1H), 7.61 (d, J = 8.5 Hz, 1H), 7.09 (d, J = 2.6 Hz, 1H), 6.67 (dd, J = 8.5, 2.6 Hz, 1H), 3.77 (s, 3H).

Synthesis of 2-ethynyl-1,3-dimethyl-1*H*-imidazol-3-ium triflate (*N*-heterocyclic allenylidene precursor)⁴



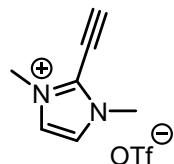
Scheme S3. The synthetic procedure of 2-ethynyl-1,3-dimethyl-1*H*-imidazol-3-ium triflate.

1-methyl-1*H*-imidazole (36.5 mmol, 3.0 g) was dissolved in THF (100 mL). n-BuLi (2.5 M in hexane, 18 mL) was added dropwisely at –78 °C. After stirring for 2 h, the temperature was raised to –60 °C and I₂ (43.8 mmol, 11.12 g) in THF (40 mL) was added slowly. The mixture was stirring at RT for another 16 h and the reaction was quenched by Na₂S₂O₃ (aq, saturated). Organic phase was collected by extraction with CH₂Cl₂ and dried over anhydrous Na₂SO₄. After evaporation under reduced pressure, the light yellow solid was collected. Recrystallization from CH₂Cl₂ and hexane gave pure 2-iodo-1-methyl-1*H*-imidazole (5.86 g). ^1H NMR (500 MHz, CD₃CN) δ 7.18 (d, J = 0.9 Hz, 1H), 6.98 (d, J = 0.9 Hz, 1H), 3.60 (s, 3H).

2-iodo-1-methyl-1*H*-imidazole (10 mmol, 2.32 g), Pd(PPh₃)₄ (0.5 mmol, 580 mg) and CuI (1 mmol, 190 mg) were dissolved in *i*-Pr₂NH (50 mL) under N₂. After degassed ethynyltriisopropylsilane (12

mmol, 2.7 mL) was added, the reaction was kept stirring at RT for 48 h under N₂ atmosphere. The filtrate was collected and concentrated to dryness. EA was added and organic phase was washed with NaCl (aq, saturated) for 3 times, dried over anhydrous Na₂SO₄. EA was evaporated and 1-methyl-2-((triisopropylsilyl)ethynyl)-1H-imidazole (1.78 g) was gained as light yellow oil after column chromatography (SiO₂, eluent: Hex : EA = 10 : 1). ¹H NMR (400 MHz, CDCl₃) δ 7.08 (d, *J* = 1.2 Hz, 1H), 6.97 (d, *J* = 1.2 Hz, 1H), 3.78 (s, 3H), 1.14 (d, *J* = 4.0 Hz, 21H).

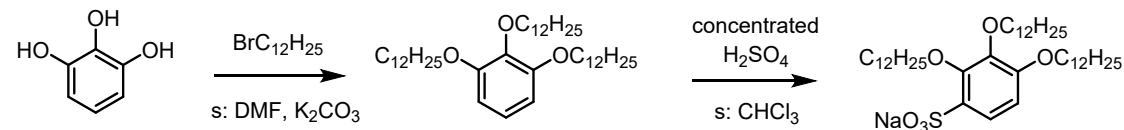
To a THF (5 mL) solution of 1-methyl-2-((triisopropylsilyl)ethynyl)-1H-imidazole (1 mmol, 262 mg), TBAF (2 mL, 1.0 mol/L in THF) was added. After the mixture was stirring at RT for 1 h, water (5 mL) was added and extracted with CH₂Cl₂ (20 mL). The organic phase was collected, washed with NaCl (aq, saturated) and dried over anhydrous Na₂SO₄. Light yellow oil collected after solvent was removed under reduced pressure at low temperature, was used directly by redissolving in CH₂Cl₂ (10 mL) at -40 °C. After methyl trifluoromethanesulfonate (excess) was added, the reaction was kept at -40 °C for 0.5 h. The target product 2-ethynyl-1,3-dimethyl-1*H*-imidazol-3-ium triflate (*N*-heterocyclic allenylidene precursor) was collected by filtration, washed with few Et₂O, dried under vacuum and stored in the fridge.



Light brown solid (120 mg).

¹H NMR (500 MHz, CD₃CN) δ 7.43 (s, 2H), 4.75 (s, 1H), 3.87 (s, 6H). IR (KBr) 2126 cm⁻¹ (C≡C).

Synthesis of the lipophilic anion (LA): sodium 2,3,4-tris(dodecyloxy)benzenesulfonate ⁵⁻⁶



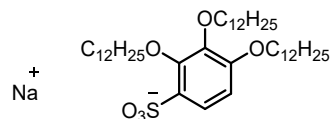
Scheme S4. The synthetic procedure of sodium 2,3,4-tris(dodecyloxy)benzenesulfonate.

NaLA was prepared according to the modified literature method.⁵⁻⁶

Pyrogallol (80 mmol, 10.1 g) and K₂CO₃ were added to DMF (125 mL) and the temperature was

raised to 60 °C. Then BrC₁₂H₂₅ (260 mmol, 62.4 mL) was added dropwisely to the system and the reaction was kept stirring at 60 °C overnight. The mixture was cooled and poured into ice water and the precipitate was collected by filtration. Nearly quantitative yield of 1,2,3-tris(dodecyloxy)benzene was obtained as pale white solid after recrystallization from acetone. ¹H NMR (500 MHz, CDCl₃) δ 6.93 (t, *J* = 8.3 Hz, 1H), 6.56 (d, *J* = 8.3 Hz, 2H), 3.98 (dt, *J* = 8.8, 6.6 Hz, 6H), 1.80 (ddd, *J* = 16.6, 14.6, 7.3 Hz, 6H), 1.53 – 1.44 (m, 6H), 1.37 – 1.25 (m, 48H), 0.90 (t, *J* = 7.0 Hz, 9H).

Concentrated H₂SO₄ (3 mL) was added to the 10 mL CHCl₃ solution of 1,2,3-tris(dodecyloxy)benzene (1.6 mmol, 1.01 g). The reaction mixture heated at 40 °C for 15 min, then slowly poured into ice water. The pH of the solution was adjusted to 12 by adding NaOH (aq) with NaCl (aq). After stirring for 0.5 h, the reaction mixture was extracted with EA (50 mL) for 3 times. The organic layer was dried over anhydrous Na₂SO₄. The organic layer was concentrated and purified by column chromatography (SiO₂) with eluent EA and EtOH subsequently. The white solid (980 mg) was obtained.



NaLA

¹H NMR (500 MHz, DMSO) δ 7.33 (d, *J* = 8.7 Hz, 1H), 6.63 (d, *J* = 8.8 Hz, 1H), 3.94 (dt, *J* = 8.4, 6.4 Hz, 4H), 3.83 (t, *J* = 6.4 Hz, 2H), 1.68 (dt, *J* = 14.5, 7.3 Hz, 6H), 1.48 – 1.38 (m, 6H), 1.25 (m, 48H), 0.85 (m, 9H).

General synthetic procedure of the tridentate cyclometallated *N*-heterocyclic allenylidene complexes⁷

PF₆ anion:

N-heterocyclic allenylidene precursor (0.16 mmol, 44 mg) and Ag₂O (0.2 mmol, 48 mg) were added to 15 mL CH₃CN and the mixture was stirred under N₂ at RT overnight, protected from light. The filtrate was collected after filtration through celite. [R(C^NN)-M-Cl] (M = Pd/Pt, 0.1 mmol) was then added to the solution. The reaction system was kept stirring under N₂ for another 12 h at RT, protected from light. Filtrate collected after filtration through celite was concentrated and

redissolved in 5 mL MeOH. The methanolic solution was added dropwisely to 20 mL saturated NH₄PF₆ (aq) and the mixture was stirred for 0.5 h. The final product was obtained after filtration and column chromatography (neutral Al₂O₃, eluent: CH₃CN).

Lipophilic anion:

Metal complexes with PF₆ counter anion (0.04 mmol) was dissolve in minimum of CH₃CN and NaLA (0.039 mmol) in CH₂Cl₂ was added. After stirring at room temperature for 2 hours, H₂O was added. The organic phase was collected, washed with H₂O three times and dried over Na₂SO₄. The final product was obtained by removing the solvent and recrystallized in hot DMSO.

Complexes characterization

Pt-1-PF₆ Green solid (yield: 80%). Orange crystals can be obtained by slow evaporation in CH₃CN solutions.

¹H NMR (500 MHz, DMSO-*d*₆) δ 8.87 (dd, *J* = 5.2, 1.5 Hz, 1H), 8.49 (d, *J* = 7.9 Hz, 1H), 8.32 (td, *J* = 7.8, 1.6 Hz, 1H), 8.22 (d, *J* = 7.8 Hz, 1H), 8.11 (t, *J* = 8.0 Hz, 1H), 8.01 (d, *J* = 8.0 Hz, 1H), 7.79 (ddd, *J* = 7.7, 5.3, 1.3 Hz, 1H), 7.66 – 7.60 (m, 3H), 7.59 – 7.52 (m, 1H), 7.13 – 7.05 (m, 2H), 3.87 (s, 6H). ¹³C NMR (126 MHz, DMSO-*d*₆) δ 163.97, 157.36, 154.51, 151.12, 147.19, 141.30, 140.73, 140.68, 137.03, 136.31, 131.78, 131.10, 128.89, 125.44, 124.47, 124.39, 121.42, 119.72, 119.64, 83.89, 35.43. ¹⁹F NMR (CD₃CN, 376 MHz) δ -72.94; ³¹P NMR (202 MHz, CD₃CN) δ -144.64; HR-MS (ESI): m/z = 546.12524, [C₂₃H₁₉N₄Pt]⁺, calc. for [C₂₃H₁₉N₄Pt]⁺ m/z = 546.1257; HR-MS (ESI): m/z = 144.96375, [PF₆]⁻, calc. for [PF₆]⁻ m/z = 144.9647. Anal. Calcd for C₂₃H₁₉N₄PtPF₆: C, 39.97; H, 2.93; N, 8.11; Found: C, 39.48; H, 2.29; N, 7.89.

Pt-1-LA Green solid (yield: 40%).

¹H NMR (400 MHz, DMSO-*d*₆) δ 8.98 (d, *J* = 4.3 Hz, 1H), 8.59 (d, *J* = 8.0 Hz, 1H), 8.41 (t, *J* = 7.9 Hz, 1H), 8.31 (d, *J* = 7.9 Hz, 1H), 8.21 (t, *J* = 8.0 Hz, 1H), 8.10 (d, *J* = 7.9 Hz, 1H), 7.91 – 7.84 (m, 1H), 7.72 (d, *J* = 7.1 Hz, 1H), 7.68 – 7.61 (m, 3H), 7.33 (d, *J* = 8.7 Hz, 1H), 7.19 – 7.09 (m, 2H), 6.63 (d, *J* = 8.8 Hz, 1H), 3.92 (m, 9H), 3.83 (t, *J* = 6.4 Hz, 3H), 1.76 – 1.58 (m, 6H), 1.25 (m, 48H), 0.85 (t, *J* = 6.7 Hz, 9H); ¹⁹F NMR (376 MHz, DMSO) no signal; ³¹P NMR (202 MHz, DMSO) no signal; HR-MS (ESI): m/z = 546.12512,

$[C_{23}H_{19}N_4Pt]^+$, calc. for $[C_{23}H_{19}N_4Pt]^+$ m/z = 546.1257; HR-MS (ESI): m/z = 709.54468,

$[C_{42}H_{77}O_6S]^-$, calc. for $[C_{42}H_{77}O_6S]^-$ m/z = 709.5446.

Pd-2-PF₆ Orange solid (yield: 38%)

¹H NMR (600 MHz, DMSO-d₆) δ 8.66 (dd, *J* = 5.2, 1.6 Hz, 1H), 8.51 (d, *J* = 8.1 Hz, 1H), 8.32 – 8.24 (m, 2H), 8.19 (t, *J* = 8.0 Hz, 1H), 7.89 (d, *J* = 8.1 Hz, 1H), 7.76 (ddd, *J* = 7.7, 5.1, 1.3 Hz, 1H), 7.64 (s, 2H), 7.15 (dd, *J* = 7.8, 2.5 Hz, 1H), 6.98 (ddd, *J* = 12.1, 9.3, 2.4 Hz, 1H), 3.87 (s, 6H). ¹³C NMR (151 MHz, DMSO-d₆) δ 159.33, 156.77, 154.11, 152.07, 145.17, 142.27, 141.34, 139.63, 132.01, 131.40, 128.61, 124.39, 123.36, 123.25, 122.09, 121.41, 121.28, 120.66, 101.53, 93.33, 84.20, 35.89. ¹⁹F NMR (CD₃CN, 376 MHz) δ -72.92, -107.52, -110.06; ³¹P NMR (202 MHz, CD₃CN) δ -144.50; IR (KBr) 2104 cm⁻¹ (C=C=C); HR-MS (ESI): m/z = 493.04538, $[C_{23}H_{17}F_2N_4Pd]^+$, calc. for $[C_{23}H_{17}F_2N_4Pd]^+$ m/z = 493.0456; HR-MS (ESI): m/z = 144.96380, $[PF_6]^-$, calc. for $[PF_6]^-$ m/z = 144.9647. Anal. Calcd for C₂₃H₁₇F₂N₄PdPF₆: C, 43.30; H, 2.68; N, 8.78; Found: C, 41.84; H, 2.51; N, 8.26.

Pd-2-LA Orange solid (yield: 53%)

¹H NMR (400 MHz, DMSO-d₆ + minor CD₂Cl₂) δ 8.76 (d, *J* = 4.5 Hz, 1H), 8.57 (d, *J* = 7.9 Hz, 1H), 8.37 – 8.29 (m, 2H), 8.24 (t, *J* = 8.1 Hz, 1H), 7.99 (d, *J* = 8.1 Hz, 1H), 7.83 – 7.77 (m, 1H), 7.62 (s, 2H), 7.37 (d, *J* = 8.7 Hz, 1H), 7.29 (d, *J* = 7.8 Hz, 1H), 6.98 – 6.92 (m, 1H), 6.60 (d, *J* = 8.8 Hz, 1H), 3.97 (dd, *J* = 12.3, 5.6 Hz, 9H), 3.86 (t, *J* = 6.4 Hz, 3H), 1.68 (dd, *J* = 14.6, 6.5 Hz, 6H), 1.25 (s, 48H), 0.86 (t, *J* = 6.7 Hz, 9H); ¹⁹F NMR (376 MHz, DMSO-d₆ + minor CD₂Cl₂) -105.91, -108.86; ³¹P NMR (202 MHz, DMSO-d₆ + minor CD₂Cl₂) no signal; HR-MS (ESI): m/z = 493.04538, $[C_{23}H_{17}N_4F_2Pd]^+$, calc. for $[C_{23}H_{17}N_4F_2Pd]^+$ m/z = 493.0456; HR-MS (ESI): m/z = 709.54435, $[C_{42}H_{77}O_6S]^-$, calc. for $[C_{42}H_{77}O_6S]^-$ m/z = 709.5446.

Pt-2-PF₆ Dark green solid (yield: 11%)

¹H NMR (500 MHz, CD₃CN) δ 8.75 (d, *J* = 5.1 Hz, 1H), 8.19 (q, *J* = 8.0 Hz, 2H), 8.03 – 7.91 (m, 2H), 7.84 (d, *J* = 7.9 Hz, 1H), 7.68 (t, *J* = 5.5 Hz, 1H), 7.34 (s, 2H), 7.02 (d, *J* = 8.4 Hz, 1H), 6.74 – 6.63 (m, 1H), 3.84 (s, 6H); ¹⁹F NMR (CD₃CN, 376 MHz) δ -72.47, -106.86, -110.46; ³¹P NMR (202 MHz, CD₃CN) δ -144.58. HR-MS (ESI): m/z = 582.10614, $[C_{23}H_{17}F_2N_4Pt]^+$, calc. for $[C_{23}H_{17}F_2N_4Pt]^+$ m/z = 582.1069; HR-MS (ESI): m/z =

144.96373, $[\text{PF}_6]^-$, calc. for $[\text{PF}_6]^-$ m/z = 144.9647. Anal. Calcd for $\text{C}_{23}\text{H}_{17}\text{F}_2\text{N}_4\text{PtPF}_6$: C, 37.99; H, 2.35; N, 7.70; Found: C, 38.50; H, 2.51; N, 6.26.

Pt-2-LA Green solid (yield: 54%)

^1H NMR (400 MHz, DMSO- d_6 + minor CD_2Cl_2) δ 8.95 (d, J = 5.2 Hz, 1H), 8.51 (t, J = 7.7 Hz, 1H), 8.38 – 8.30 (m, 1H), 8.25 (t, J = 8.1 Hz, 1H), 8.15 (dd, J = 14.7, 7.8 Hz, 1H), 8.00 (d, J = 8.1 Hz, 1H), 7.87 – 7.77 (m, 1H), 7.54 (d, J = 7.7 Hz, 2H), 7.43 (d, J = 8.6 Hz, 1H), 7.24 (d, J = 8.6 Hz, 1H), 6.80 – 6.70 (m, 1H), 6.61 – 6.51 (m, 1H), 4.22 – 3.58 (m, 12H), 1.75 (s, 6H), 1.26 (s, 48H), 0.86 (q, J = 3.4 Hz, 9H); ^{19}F NMR (376 MHz, DMSO- d_6 + minor CD_2Cl_2) –105.60, –109.54; ^{31}P NMR (202 MHz, DMSO) no signal; HR-MS (ESI): m/z = 582.10614, $[\text{C}_{23}\text{H}_{17}\text{N}_4\text{F}_2\text{Pt}]^+$, calc. for $[\text{C}_{23}\text{H}_{17}\text{F}_2\text{N}_4\text{Pt}]^+$ m/z = 582.1069; HR-MS (ESI): m/z = 709.54475, $[\text{C}_{42}\text{H}_{77}\text{O}_6\text{S}]^-$, calc. for $[\text{C}_{42}\text{H}_{77}\text{O}_6\text{S}]^-$ m/z = 709.5446.

Pd-3-PF₆ Orange solid (yield: 45%)

^1H NMR (600 MHz, DMSO- d_6) δ 8.70 (d, J = 5.0 Hz, 1H), 8.50 (d, J = 8.0 Hz, 1H), 8.27 (t, J = 7.9 Hz, 1H), 8.11 (dt, J = 15.6, 7.8 Hz, 2H), 7.90 (d, J = 7.8 Hz, 1H), 7.75 (t, J = 6.5 Hz, 1H), 7.66 (d, J = 8.7 Hz, 1H), 7.62 (s, 2H), 7.17 (s, 1H), 6.68 (dd, J = 8.6, 2.3 Hz, 1H), 3.88 (s, 6H), 3.77 (s, 3H). ^{13}C NMR (151 MHz, DMSO- d_6) δ 162.25, 159.67, 155.92, 155.61, 152.74, 151.13, 147.11, 140.73, 140.62, 140.33, 130.84, 127.53, 126.24, 123.66, 123.21, 121.15, 118.97, 118.33, 109.94, 83.65, 54.73, 35.07. ^{19}F NMR (376 MHz, CD_3CN) δ –72.90; ^{31}P NMR (202 MHz, CD_3CN) δ –144.63. IR (KBr) 2098 cm^{-1} (C=C=C); HR-MS (ESI): m/z = 487.07468, $[\text{C}_{24}\text{H}_{21}\text{N}_4\text{OPd}]^+$, calc. for $[\text{C}_{24}\text{H}_{21}\text{N}_4\text{OPd}]^+$ m/z = 487.0750; HR-MS (ESI): m/z = 144.96374, $[\text{PF}_6]^-$, calc. for $[\text{PF}_6]^-$ m/z = 144.9647. Anal. Calcd for $\text{C}_{24}\text{H}_{21}\text{N}_4\text{OPdPF}_6$: C, 45.61; H, 3.34; N, 8.86; Found: C, 44.76; H, 3.19; N, 8.66.

Pd-3-LA Red solid (yield: 51%). Red solid turned orange when fumed with methanol vapor.

^1H NMR (500 MHz, DMSO- d_6) δ 8.75 (d, J = 5.3 Hz, 1H), 8.52 (d, J = 8.0 Hz, 1H), 8.31 (d, J = 7.8 Hz, 1H), 8.14 (d, J = 9.0 Hz, 2H), 7.94 (d, J = 7.4 Hz, 1H), 7.79 (t, J = 6.5 Hz, 1H), 7.70 (d, J = 8.6 Hz, 1H), 7.61 (s, 2H), 7.33 (d, J = 8.7 Hz, 1H), 7.23 (d, J = 2.5 Hz, 1H), 6.72 (d, J = 8.9 Hz, 1H), 6.64 (d, J = 8.8 Hz, 1H), 3.95 – 3.93 (m, 4H), 3.89 (s, 6H), 3.83 (m, 2H), 3.78 (s, 3H), 1.68 (dt, J = 14.8, 7.4 Hz, 6H), 1.24 (m, 48H), 0.85 (t, J = 6.6 Hz, 9H). ^{19}F NMR (376 MHz, DMSO- d_6) no signal; ^{31}P NMR (202 MHz, DMSO- d_6) no signal; HR-MS

(ESI): m/z = 487.07462, [C₂₄H₂₁N₄OPd]⁺, calc. for [C₂₄H₂₁N₄OPd]⁺ m/z = 487.0750; HR-MS (ESI): m/z = 709.54456, [C₄₂H₇₇O₆S]⁻, calc. for [C₄₂H₇₇O₆S]⁻ m/z = 709.5446.

Pt-3-PF₆ Green solid (yield: 32%)

¹H NMR (500 MHz, DMSO-*d*₆) δ 8.79 (dd, *J* = 5.1, 1.5 Hz, 1H), 8.45 (d, *J* = 8.0 Hz, 1H), 8.27 (td, *J* = 7.8, 1.6 Hz, 1H), 8.08 (d, *J* = 7.8 Hz, 1H), 7.97 (t, *J* = 8.0 Hz, 1H), 7.83 (d, *J* = 8.0 Hz, 1H), 7.74 (ddd, *J* = 7.7, 5.3, 1.3 Hz, 1H), 7.62 (s, 2H), 7.55 (d, *J* = 8.6 Hz, 1H), 6.99 (d, *J* = 2.6 Hz, 1H), 6.61 (dd, *J* = 8.5, 2.6 Hz, 1H), 3.85 (s, 6H), 3.75 (s, 3H). ¹³C NMR (126 MHz, DMSO-*d*₆) δ 164.31, 161.38, 157.93, 154.68, 151.50, 143.45, 141.24, 140.90, 139.91, 137.00, 132.21, 129.07, 127.44, 124.64, 122.25, 121.84, 119.29, 118.72, 110.04, 83.73, 55.34, 35.80. ¹⁹F NMR (376 MHz, CD₃CN) δ -72.95; ³¹P NMR (202 MHz, CD₃CN) δ -144.64; HR-MS (ESI): m/z = 576.13562, [C₂₄H₂₁N₄OPt]⁺, calc. for [C₂₄H₂₁N₄OPt]⁺ m/z = 576.1363; HR-MS (ESI): m/z = 144.96371, [PF₆]⁻, calc. for [PF₆]⁻ m/z = 144.9647. Anal. Calcd for C₂₄H₂₁N₄OPtPF₆: C, 39.97; H, 2.93; N, 7.77; Found: C, 39.46; H, 2.59; N, 7.60.

Pt-3-LA Red or green solid (yield: 30%). Green solid turned red when fumed with methanol vapor.

¹H NMR (400 MHz, CD₂Cl₂) δ 8.96 (s, 1H), 8.23 – 8.17 (m, 1H), 8.12 (d, *J* = 7.5 Hz, 1H), 7.91 (t, *J* = 7.8 Hz, 1H), 7.74 (dd, *J* = 13.1, 7.4 Hz, 2H), 7.56 (dd, *J* = 13.1, 8.3 Hz, 2H), 7.44 (d, *J* = 8.5 Hz, 1H), 7.38 (s, 2H), 7.19 (d, *J* = 2.6 Hz, 1H), 6.68 (d, *J* = 8.5 Hz, 1H), 6.60 (d, *J* = 8.6 Hz, 1H), 4.25 – 4.02 (m, 4H), 3.98 (s, 8H), 3.84 (s, 3H), 1.83 (d, *J* = 7.7 Hz, 6H), 1.30 (d, *J* = 9.3 Hz, 48H), 0.99 – 0.83 (m, 9H); ¹⁹F NMR (376 MHz, DMSO) no signal; ³¹P NMR (202 MHz, DMSO) no signal; HR-MS (ESI): m/z = 576.13550, [C₂₄H₂₁N₄OPt]⁺, calc. for [C₂₄H₂₁N₄OPt]⁺ m/z = 576.1363; HR-MS (ESI): m/z = 709.54448, [C₄₂H₇₇O₆S]⁻, calc. for [C₄₂H₇₇O₆S]⁻ m/z = 709.5446.

Table S1. Crystal Data for **Pd-1-PF₆** (yellow block),⁷ **Pt-1-PF₆** and **Pd-3-LA·CH₂Cl₂**.

	Pd-1-PF₆-yellow	Pt-1-PF₆	Pd-3-LA·CH₂Cl₂
formula	C ₂₃ H ₁₉ F ₆ N ₄ P Pd	C ₂₃ H ₁₉ F ₆ N ₄ P Pt	C ₆₇ H ₁₀₀ Cl ₂ N ₄ O ₇ PdS
fw	602.79	691.48	1282.86
color	yellow	orange	orange
crystal size (mm)	0.40 × 0.32 × 0.28	0.42 × 0.32 × 0.28	0.36 × 0.32 × 0.08
crystal system	<i>P</i> -1	<i>P</i> -1	<i>P</i> 1 2 ₁ 1
space group	triclinic	triclinic	monoclinic
<i>a</i> , Å	8.2664(11)	8.2935(4)	8.3719(2)
<i>b</i> , Å	11.9680(15)	11.9546(6)	58.8373(16)
<i>c</i> , Å	12.4012(16)	12.3936(6)	13.8630(4)
<i>α</i> , deg	73.332(4)	73.231(2)	90
<i>β</i> , deg	73.511(4)	73.486(2)	90.4740(10)
<i>γ</i> , deg	74.085(4)	73.658(2)	90
<i>V</i> , Å ³	1101.9(2)	1101.06(10)	6828.4(3)
<i>Z</i>	2	2	4
<i>D_c</i> , g cm ⁻³	1.817	2.086	1.248
<i>μ</i> , mm ⁻¹	0.986	6.516	3.606
<i>F</i> (000)	600	664	2728
2 <i>θ</i> _{max} , deg	27.533	45.107	68.357
no. reflections	11570	113825	82855
no. independent reflections	5010 [R _{int} = 0.0596]	18171 [R _{int} = 0.0408]	24494 [R _{int} = 0.0494]
no. variables	319	319	1491
GOF on F ²	1.035	1.103	1.065
R ₁ ^a	0.0314	0.0345	0.0460
wR ₂ ^b	0.0799	0.0793	0.1140
residual ρ, eÅ ⁻³	+0.693, -0.525	+6.049, -4.584	+0.855, -1.298

^a R = Σ||F_o|-|F_c||/Σ|F_o|. ^b R_w = {Σ[w(F_o²-F_c²)²]/Σ[w(F_o²)²]})^{1/2}.

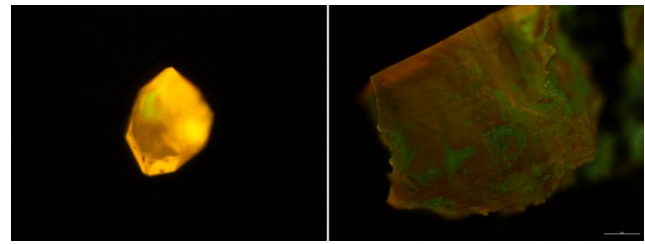


Figure S1 Micrographs of crystals of **Pt-1-PF₆** (left) and **Pd-3-LA·CH₂Cl₂** (right) under a fluorescence microscope (excitation @ 365 nm).

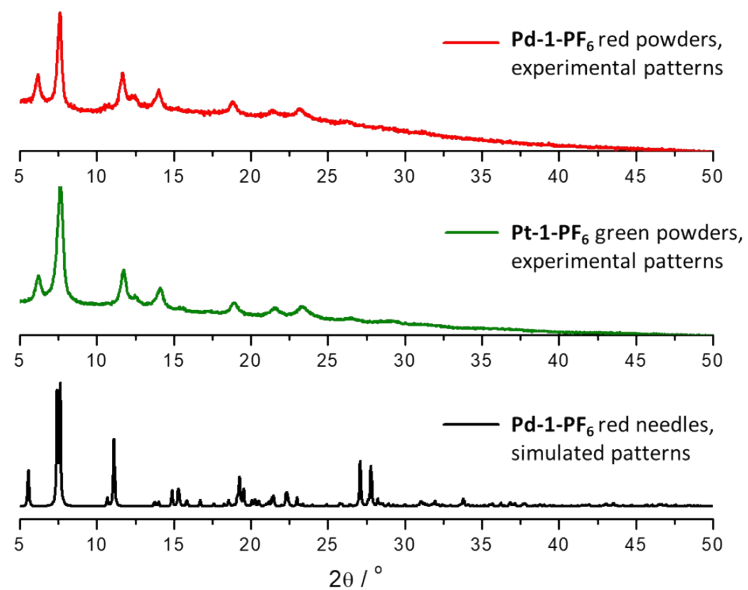


Figure S2. Experimental and simulated powder X-ray diffraction patterns for bulky red **Pd-1-PF₆** red powders (red line), **Pt-1-PF₆** green powders (green line) and red needle-like **Pd-1-PF₆** single crystals (black line) respectively.

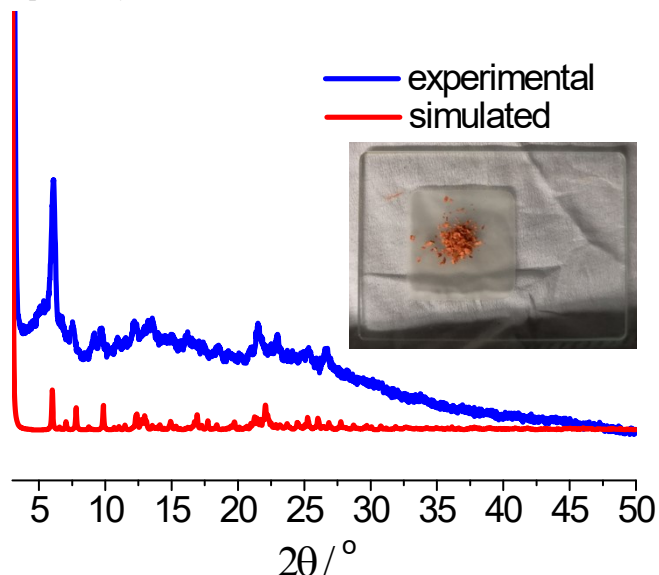


Figure S3. Experimental (blue line) and simulated (red line) powder X-ray diffraction patterns for bulky orange **Pd-3-LA** powder and **Pd-3-LA·CH₂Cl₂** single X-ray crystal structure respectively. Inset: image of bulky orange **Pd-3-LA** powder for the PXRD test.

Table S2. Photophysical Data.

Complex	Medium (T / K), (10^{-5} M)	λ_{abs} / nm ($\varepsilon / \times 10^3 \text{ mol}^{-1}\text{dm}^3\text{cm}^{-1}$)	λ_{em} / nm ($\tau / \mu\text{s}$)	Φ_{em}
Pd-1-PF₆⁷	CH ₃ CN (298)	264 (35.9), 280 (39.8), 319 (18.8), 333 (15.2)	Non-emissive	-- ^a
	butyronitrile (77) (1.6×10^{-4} M)	-- ^a	570 (13.0)	>0.99
	Solid (298)	-- ^a	695 (1.20)	0.43
Pd-1-LA⁷	CH ₂ Cl ₂ (298)	269 (33.3), 281 (35.4), 320 (16.4), 337 (12.6)	Non-emissive	-- ^a
	Toluene (298)	291 (14.1), 332 (8.9), 346 (9.7), 528 (3.7)	610 (0.26)	0.14
	Solid (298)	-- ^a	Yellow: 550 (0.48), Red: 630 (0.45)	0.14, 0.46
Pd-2-PF₆	CH ₃ CN (298)	255 (33.7), 278 (39.5), 309 (16.1), 396 (1.0)	Non-emissive	-- ^a
	butyronitrile (77)	-- ^a	602 (12.4)	-- ^a
	Solid (298)	-- ^a	Orange: 605 (0.42)	0.38
Pd-2-LA	CH ₂ Cl ₂ (298)	261 (45.0), 271 (45.2), 279 (48.9), 314 (17.0), 329 (12.8), 403 (2.0)	Non-emissive	-- ^a
	Toluene (298)	299 (20.4), 329 (7.0), 374 (3.4), 513 (2.1)	660 (0.58)	0.45
	Solid (298)	-- ^a	Orange: 586 (0.32)	0.17
Pd-3-PF₆	CH ₃ CN (298)	263 (41.0), 286 (41.7), 315 (21.6), 407 (2.0)	Non-emissive	-- ^a
	butyronitrile (77)	-- ^a	502 (162.0), (165.0), 607 (33.2)	-- ^a
	Solid (298)	-- ^a	Orange: 625 (1.71)	0.21
Pd-3-LA	CH ₂ Cl ₂ (5×10^{-5} M)	266 (21.4), 287 (21.7), 318 (11.0), 410 (1.1)	Non-emissive	-- ^a
	Toluene (298) (5×10^{-5} M)	296 (8.4), 346 (5.7), 520 (2.1)	600, 680 (0.26)	0.04
	Solid (298)	-- ^a	Orange: 588 (5.0), Red: 625 (0.37)	0.13, 0.12
Pt-1-PF₆	CH ₃ CN (298)	278 (37.4), 332 (15.8), 353 (12.4), 403 (5.9)	563 (0.30) ^b	0.04 ^b
	butyronitrile (77)	-- ^a	515 (5.8), 553, 600	-- ^a
	Solid (298)	-- ^a	Green: 830 ^c	< 0.01
Pt-1-LA	CH ₂ Cl ₂ (298)	278 (37.2), 325 (15.4), 359 (12.4), 413 (5.0)	550 (0.56) ^b , 580	0.06 ^b
	Toluene (298)	287 (20.8), 368 (6.7), 432 (3.2), 750 (2.2)	875 ^c	< 0.01

	Solid (298)	-- ^a	Green: 958 ^c	< 0.01
Pt-2-PF₆	CH ₃ CN (298)	273 (28.2), 281 (28.6), 319 (11.4),	521 (0.02) ^b , 545	0.01 ^b
		336 (9.2), 352 (7.2), 401 (4.3)		
	butyronitrile (77)	-- ^a	496 (6.1), 532 (6.2),	-- ^a
			573 (6.4), 679 (2.5)	
	Solid (298)	-- ^a	850 ^c	< 0.01
Pt-2-LA	CH ₂ Cl ₂ (298)	274 (34.2), 283 (33.6), 321 (13.2),	521 (2.0) ^b , 552 (2.0) ^b	0.2 ^b
		339 (10.9), 356 (8.6), 390 (4.6), 406 (4.5)		
	Toluene (298)	315 (5.8), 329 (5.4), 345 (4.7), 397 (3.0), 725 (2.7)	860 (0.03)	0.02
	Solid (298)	-- ^a	870 ^c	< 0.01
Pt-3-PF₆	CH ₃ CN (298)	287 (40.86), 347 (15.1), 406 (5.3)	600 (0.80) ^b	0.04 ^b
		butyronitrile (77)	-- ^a	545 (7.3), 580, 675
	Solid (298)	-- ^a	840 ^c	< 0.01
Pt-3-LA	CH ₂ Cl ₂ (298) (5 × 10 ⁻⁵ M)	291 (54.3), 354 (20.9), 411 (5.8)	620 (0.29) ^b	0.02 ^b
		Toluene (298) (5 × 10 ⁻⁵ M)	303 (10.8), 369 (5.5), 720 (3.0)	875 ^c
	Solid (298)	-- ^a	Red: 715 (0.52), Green: 895 ^c	Red: 0.07, Green: < 0.01

^aNo detection. ^bThe data were collected in solutions degassed by N₂ bubbling. ^cLifetimes were not obtained due to the weak emission intensity.

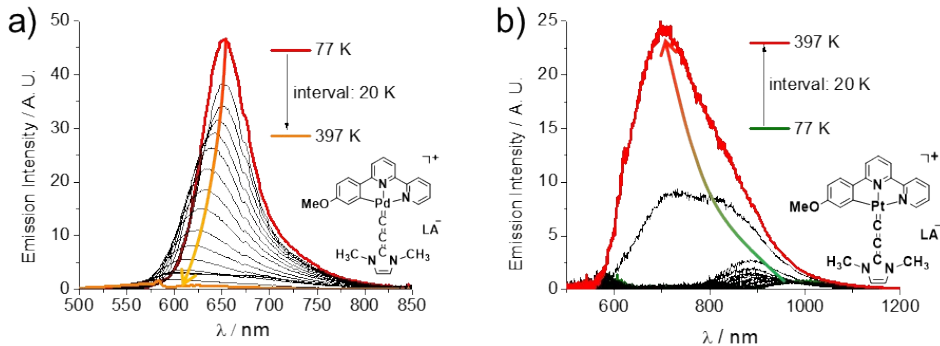


Figure S4. Solid-state emission spectra of a) **Pd-3-LA** (red solid, $\lambda_{\text{ex}} = 470 \text{ nm}$) and b) **Pt-3-LA** (green solid, $\lambda_{\text{ex}} = 470 \text{ nm}$) at variable temperatures.

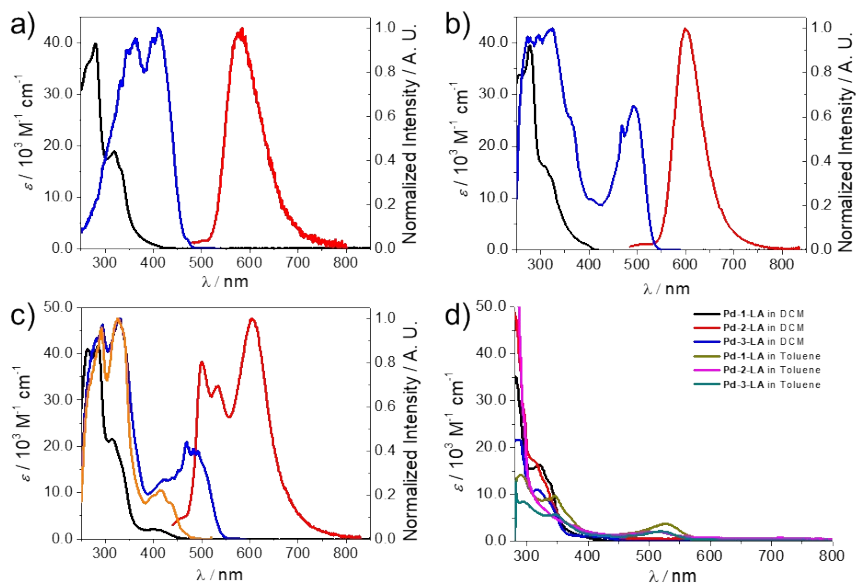


Figure S5 a-c) Electronic absorption (black line) of **Pd-(1-3)-PF₆** in room temperature CH₃CN, normalized excitation (blue and orange line) and emission (red line) spectra of **Pd-(1-3)-PF₆** in CH₃CH₂CH₂CN at 77 K. d) Electronic absorption spectra of **Pd-(1-3)-LA** at room temperature in CH₂Cl₂ and toluene respectively.

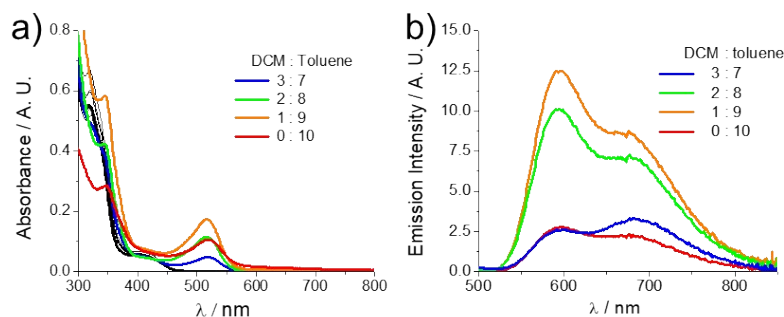


Figure S6. a) Absorption and b) emission ($\lambda_{\text{ex}} = 400 \text{ nm}$) spectra **Pd-3-LA** in CH₂Cl₂/toluene solutions with a variety volumetric ratios (10/0 ~ 0/10) at 298 K (concentration $\sim 5.0 \times 10^{-5} \text{ M}$).

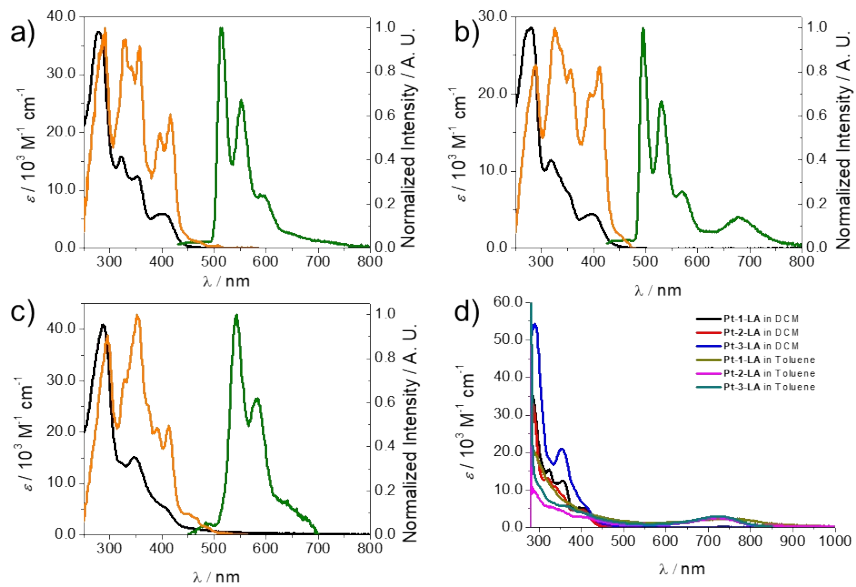


Figure S7 a-c) Electronic absorption (black line) of **Pt-(1-3)-PF₆** in room temperature CH₃CN, normalized excitation (orange line) and emission (green line) spectra of **Pt-(1-3)-PF₆** (1.0×10^{-5} M) in CH₃CH₂CH₂CN at 77 K. d) Electronic absorption spectra of **Pt-(1-3)-LA** at room temperature in CH₂Cl₂ and toluene respectively.

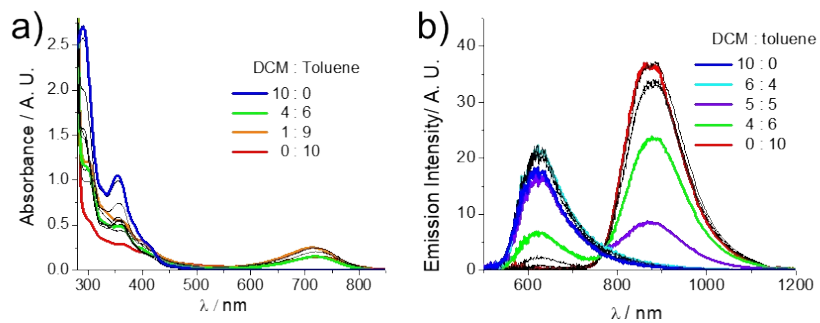
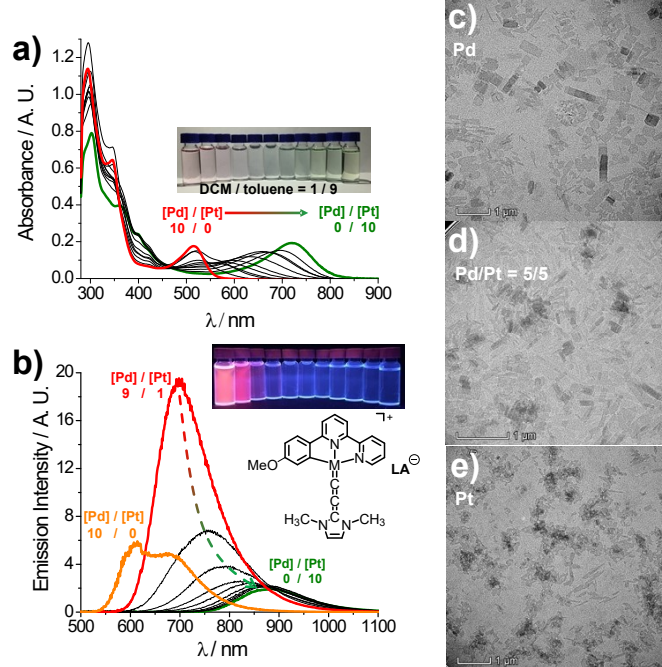
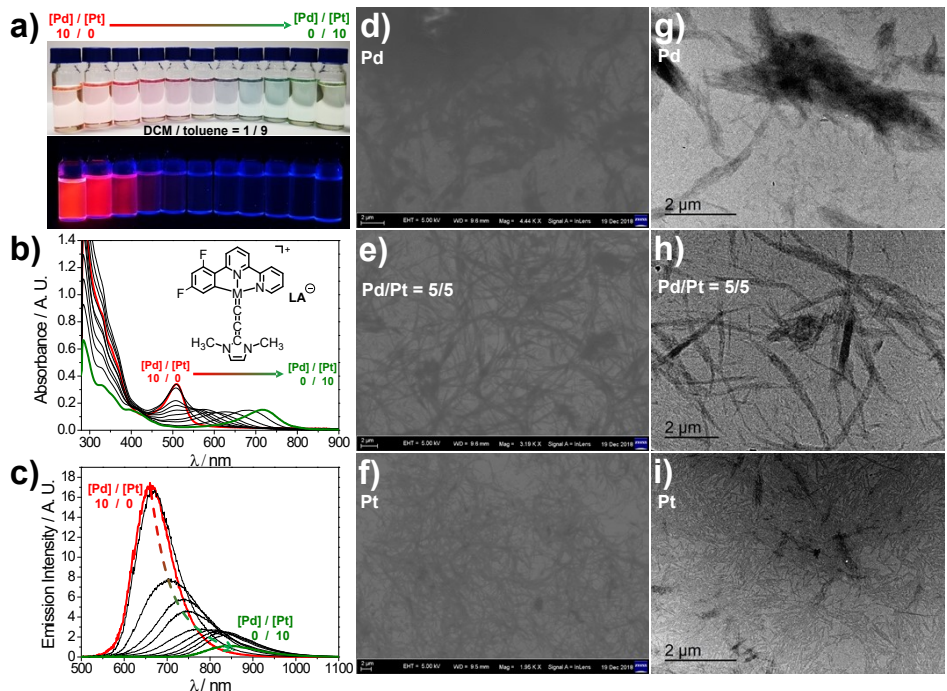


Figure S8. a) Absorption and b) emission ($\lambda_{\text{ex}} = 425$ nm) spectra **Pt-3-LA** in CH₂Cl₂/toluene solutions with a variety volumetric ratios (10/0 ~ 0/10) at 298 K (concentration $\sim 5.0 \times 10^{-5}$ M).



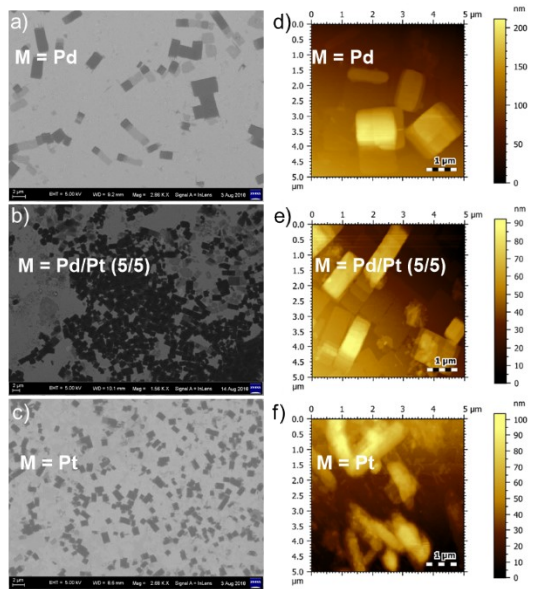


Figure S11. a-c) SEM and d-f) AFM images of **M(Pd/Pt)-1-LA** (5.0×10^{-5} M) in $\text{CH}_2\text{Cl}_2/\text{toluene}$ (1/9) solutions.

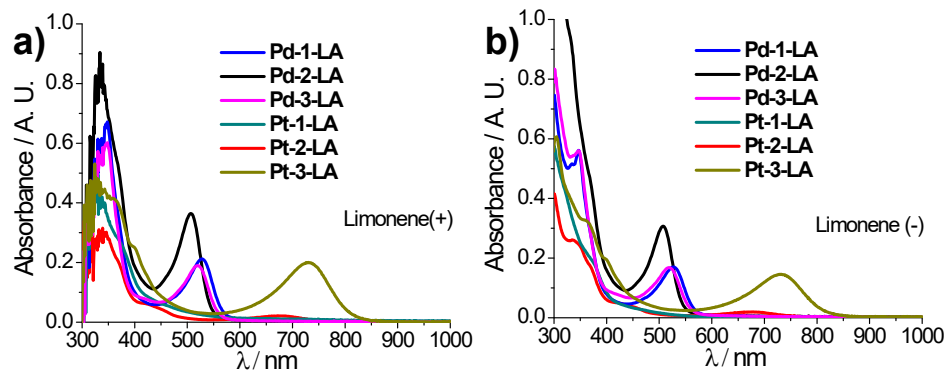


Figure S12. UV-vis absorption spectra after 2 h stirring in $\text{CH}_2\text{Cl}_2/\text{limonene}$ (1/9) solutions (5×10^{-5} M) for **Pd-1-LA** (blue line), **Pd-2-LA** (black line), **Pd-3-LA** (purple line), **Pt-1-LA** (green line), **Pt-2-LA** (red line) and **Pt-3-LA** (dark yellow line), respectively. Chiral solvent used: a) limonene (+), b) limonene (-).

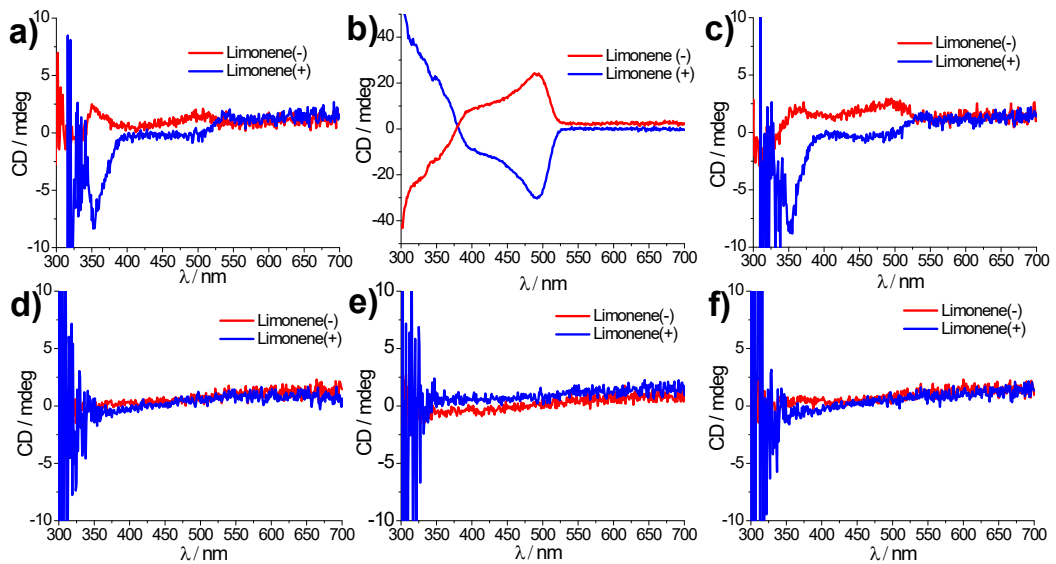


Figure S13. CD spectra after 2 h stirring in $\text{CH}_2\text{Cl}_2/\text{limonene}$ (1/9) solutions (limonene (+): blue line, limonene (-): red line) for a) **Pd-1-LA** (5.0×10^{-5} M), b) **Pd-2-LA** (2.5×10^{-5} M), c) **Pd-3-LA** (5.0×10^{-5} M), d) **Pt-1-LA** (5.0×10^{-5} M), e) **Pt-2-LA** (5.0×10^{-5} M) and **Pt-3-LA** (5.0×10^{-5} M), respectively.

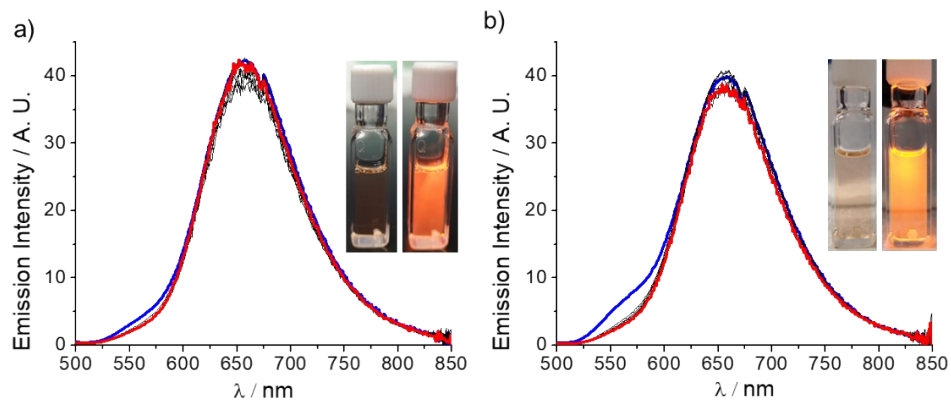


Figure S14. Time-dependent emission spectra (inset: sample images under ambient light (left) and 365 nm UV light (right) respectively) of **Pd-2-LA** (2.5×10^{-5} M) in $\text{CH}_2\text{Cl}_2/\text{limonene}$ (1/9) solution: a) limonene (+), b) limonene (-).

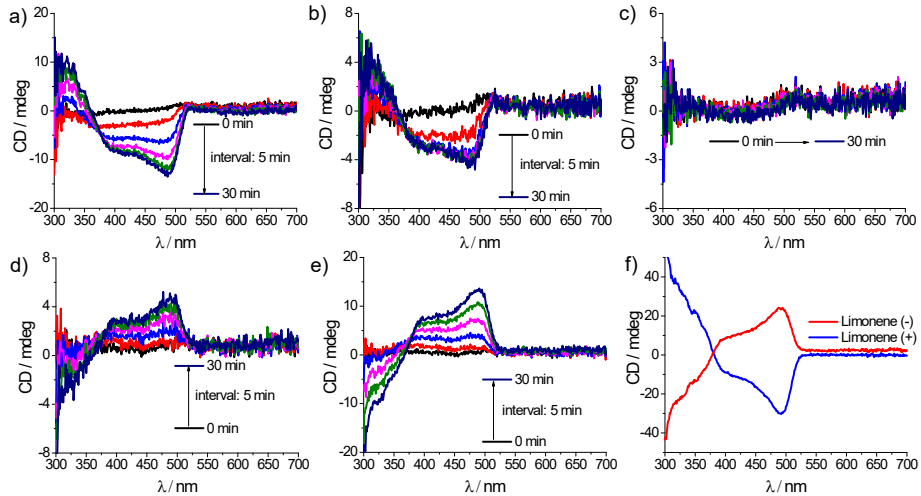


Figure S15. Time-dependent CD spectra of **Pd-2-LA** (2.5×10^{-5} M) in $\text{CH}_2\text{Cl}_2/\text{limonene}$ (1/9) solutions with various optical rotations: a) limonene (+), b) limonene (+) / limonene (-) = 2/1, c) limonene (racemic), d) limonene (+) / limonene (-) = 1/2, e) limonene (-). f) Terminal state of the CD spectra after 2 h stirring in $\text{CH}_2\text{Cl}_2/\text{limonene}$ (1/9) solutions (limonene (-): blue, limonene (+): red).

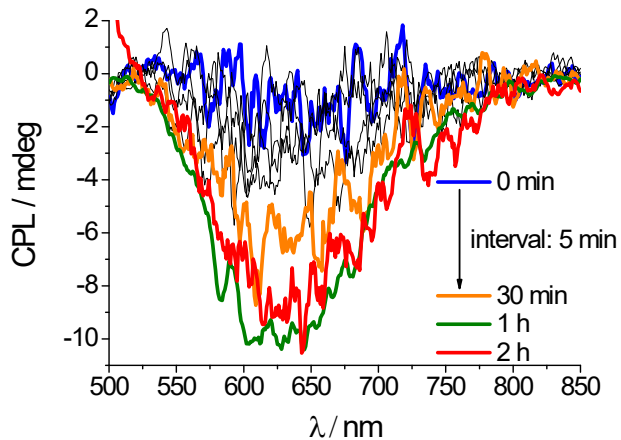


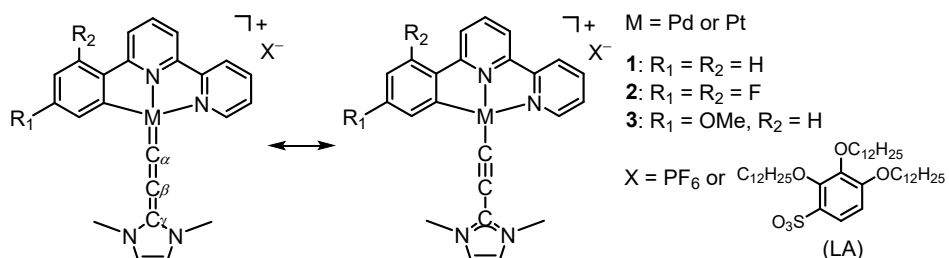
Figure S16. Time-dependent CPL spectra of **Pd-2-LA** (2.5×10^{-5} M) in $\text{CH}_2\text{Cl}_2/\text{limonene}$ (+, 1/9) solution.

The vortex effect on the chiral signals have also been considered. The stirring speed and CW (clockwise)-CCW (counter clockwise) operation of the stirring bars have no influence on the dilute solutions, but did have great impacts on the CD and CPL values for the samples containing **Pd-2-LA** higher than 5.0×10^{-5} M in homochiral $\text{CH}_2\text{Cl}_2/\text{limonene}$ (1/9) solutions. The time-dependent and semi-reversible g_{CD} and g_{lum} values changes, before and after stirring (CW/CCW), with or without stirring (CW/CCW), remained unexplained and should be a future issue.

Table S3. Characteristic survey of the allenylidene properties.

	^{13}C -NMR chemical shift (C_β) / ppm	$\nu(\text{C}=\text{C}=\text{C})$ / cm^{-1}	$\text{C}_\alpha-\text{C}_\beta$ / Å
Pd-1-PF₆	83.9	2104 (red)	1.214 (yellow), 1.188 (red)
Pt-1-PF₆	83.9	-- ^a	1.225 (orange)
Pd-2-PF₆	84.2	2104 (orange)	-- ^a
Pd-3-PF₆	83.6	2098 (red)	1.221 (orange, -LA)

^a Not detected.



Scheme S5. Mesomerism between cyclometallated tridentate metal allenylidene and zwitterionic acetylide.

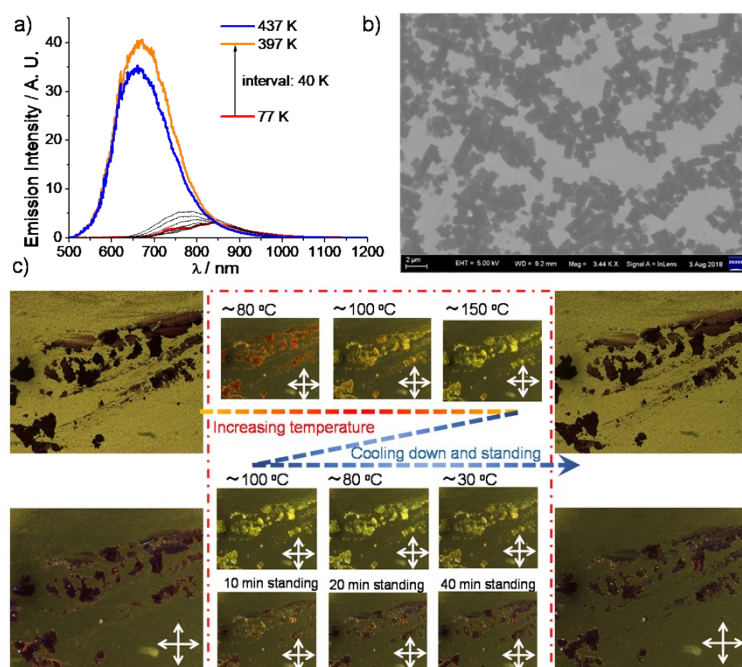


Figure S17. a) Temperature dependent solid emission spectra, b) SEM image and c) the heating and cooling cycle of **M-1-LA** (M: Pd/Pt = 8/2) obtained from the mixed solution of CH_2Cl_2 /Toluene (1/9, total metal concentration = 3.5×10^{-4} M) under POM.

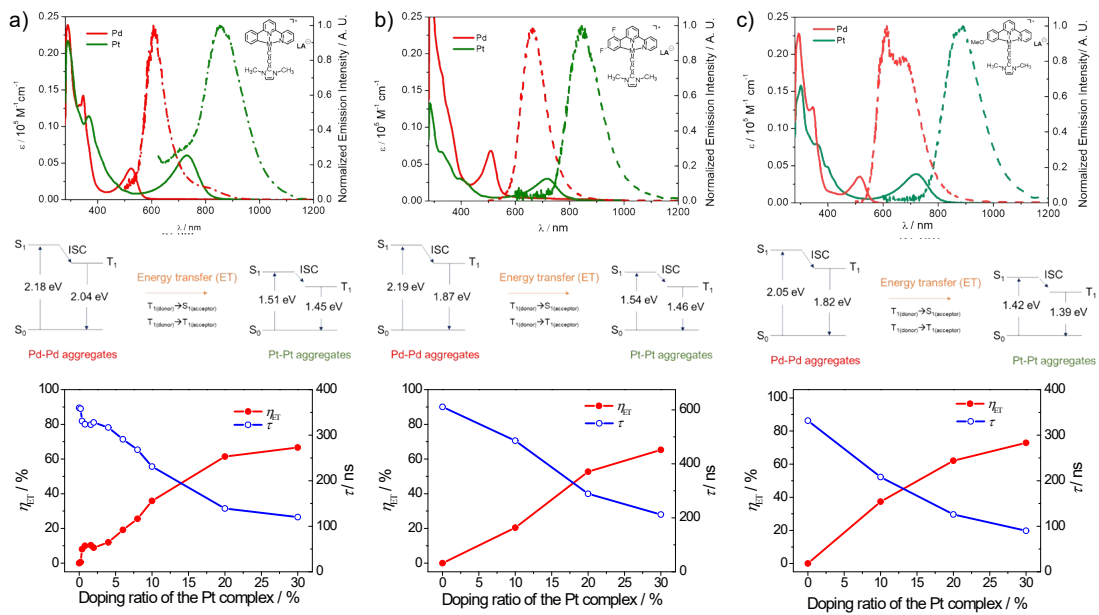


Figure S18. Top: UV-vis absorption (solid line) and emission (dashed line) spectra of a) **Pd-1-LA** (red) and **Pt-1-LA** (green), b) **Pd-2-LA** (red) and **Pt-2-LA** (green), c) **Pd-3-LA** (red) and **Pt-3-LA** (green) in solution ($\text{CH}_2\text{Cl}_2/\text{Toluene} = 1/9$, 5.0×10^{-5} M). **Middle:** energy diagram of donor and acceptor. ET=energy transfer, ISC=intersystem crossing. **Bottom:** Plots of the energy transfer efficiency (η_{ET}) and lifetime (τ) at the donor emission wavelength as a function of the doping ratio of the Pt congeners in the mixed aggregates.

Table S4. Lifetimes of the mixed component **M(Pd/Pt)-1-LA** (total metal concentration: 5×10^{-5} M) recorded @ em 695 nm in solution ($\text{CH}_2\text{Cl}_2/\text{Toluene} = 1/9$) at room temperature, and corresponding parameters calculated for the energy transfer process.

Pt (%)	0	0.2	0.4	0.8	1.6	2	4	6	8	10	20	30
τ (ns)	360	358	331	324	323	328	317	291	268	231	139	120
η_{ET} (%)	--	0.56	8.06	10.00	10.28	8.89	11.94	19.17	25.56	35.83	61.39	66.67
k_{total} ($\times 10^6$ s ⁻¹)	2.78	2.79	3.02	3.09	3.10	3.05	3.15	3.44	3.73	4.33	7.19	8.33
k_{ET} ($\times 10^6$ s ⁻¹)	--	0.02	0.24	0.31	0.32	0.27	0.38	0.66	0.95	1.55	4.42	5.56

Table S5. Lifetimes of the mixed component **M(Pd/Pt)-2-LA** (total metal concentration: 5×10^{-5} M) recorded @ em 662 nm in solution ($\text{CH}_2\text{Cl}_2/\text{Toluene} = 1/9$) at room temperature, and corresponding parameters calculated for the energy transfer process.

Pt (%)	0	10	20	30
τ (ns)	611	486	289	212
η_{ET} (%)	--	20.46	52.70	65.30
k_{total} ($\times 10^6$ s ⁻¹)	1.64	2.06	3.46	4.72
k_{ET} ($\times 10^6$ s ⁻¹)	--	0.42	1.82	3.08

Table S6. Lifetimes of the mixed component **M(Pd/Pt)-3-LA** (total metal concentration: 5×10^{-5} M) recorded in solution ($\text{CH}_2\text{Cl}_2/\text{Toluene} = 1/9$) at room temperature, and corresponding parameters calculated for the energy transfer process.

Pt (%)	0	10	20	30
τ (ns)	332	208	126	90
η_{ET} (%)	--	37.35	62.05	72.89
k_{total} ($\times 10^6$ s $^{-1}$)	3.01	4.81	7.94	11.11
k_{ET} ($\times 10^6$ s $^{-1}$)	--	1.80	4.92	8.10

τ : lifetetime; τ_{DA} : lifetime recorded with specific doping of the Pt acceptors; τ_D : lifetime of Pd donor.

k_{ET} : energy transfer rate. $k_{ET}=k_{total}-(k_r+k_{nr})=1/\tau_{DA}-1/\tau_D$.

η_{ET} : energy transfer efficiency. $\eta_{ET}=1-\tau_{DA}/\tau_D$.

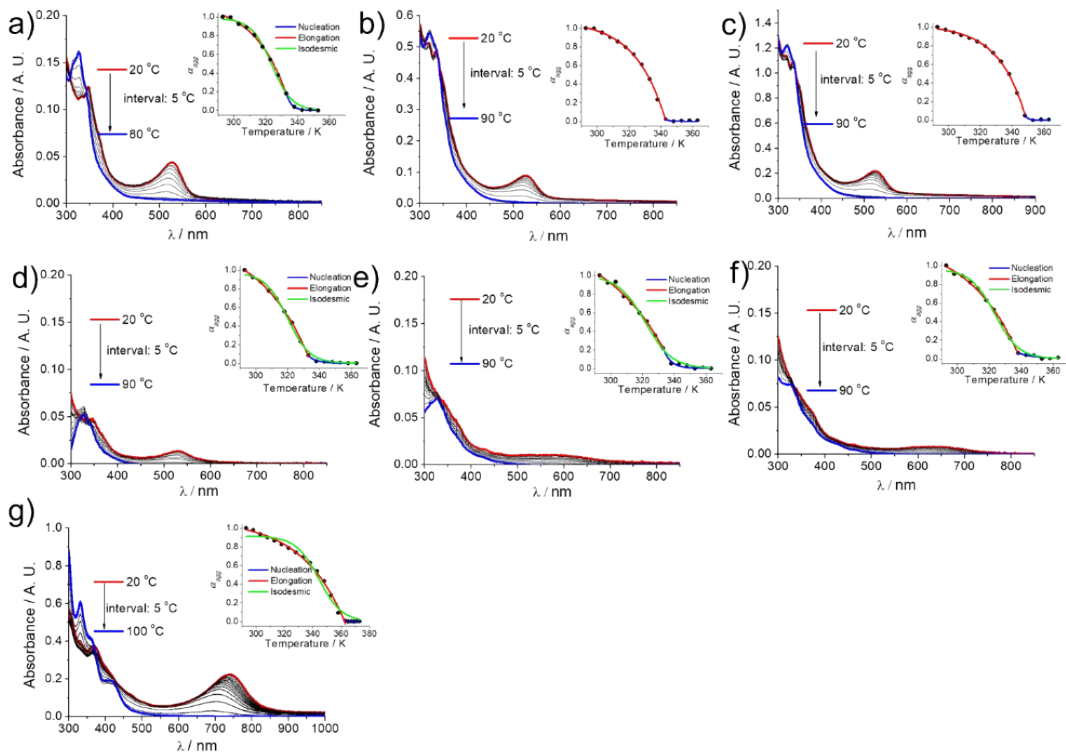


Figure S19. Temperature dependent UV-vis absorption of **Pd-1-LA** in toluene solutions with various concentrations: a) 1.0×10⁻⁵ M, b) 2.5×10⁻⁵ M, c) 5.0×10⁻⁵ M. UV-vis absorption of mixed **M(Pd/Pt)-1-LA** aggregates with different Pd/Pt ratio recorded in toluene solutions by increasing the temperatures: d) M = Pd/Pt (8/2) (1.0×10⁻⁵ M), e) M = Pd/Pt (5/5) (1.0×10⁻⁵ M), f) M = Pd/Pt (2/8) (1.0×10⁻⁵ M), g) M = Pt (5.0×10⁻⁵ M). (Inset: data plot for the degree of aggregation against temperature, and corresponding fitting results with both cooperative nucleation-elongation (blue-red line) and isodesmic (green line) models respectively).

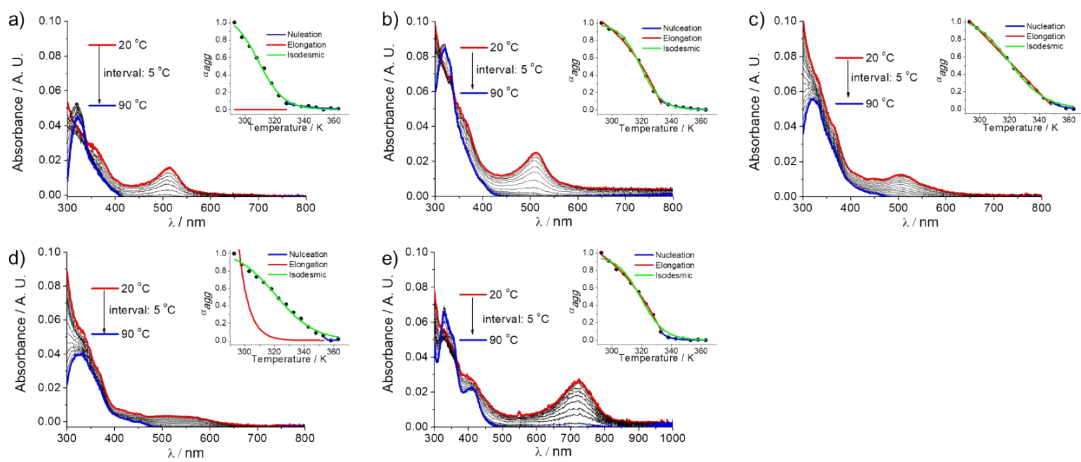


Figure S20. UV-vis absorption of **M(Pd/Pt)-2-LA** (1.0×10⁻⁵ M) recorded in toluene solutions by increasing the temperatures: a) M = Pd, b) M = Pd/Pt (8/2), c) M = Pd/Pt (5/5), d) M = Pd/Pt (2/8), M = Pt. (Inset: data plot for the degree of aggregation against temperature, and corresponding fitting results with both cooperative nucleation-elongation and isodesmic models respectively).

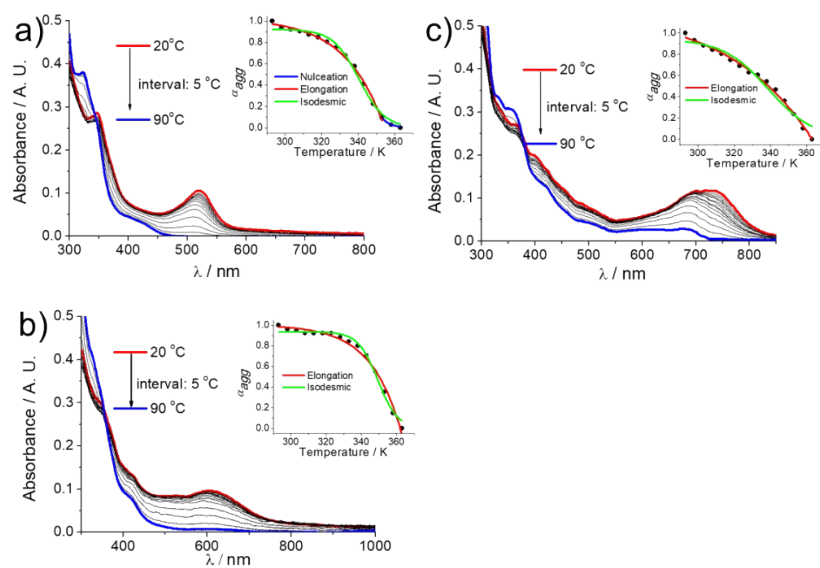


Figure S21. UV-vis absorption of **M(Pd/Pt)-3-LA** (5.0×10^{-5} M) recorded in toluene solutions by increasing the temperatures: a) $M = \text{Pd}$, b) $M = \text{Pd/Pt} (5/5)$, c) $M = \text{Pt}$. (Inset: data plot for the degree of aggregation against temperature, and corresponding fitting results with both cooperative nucleation-elongation and isodesmic models respectively).

Table S7. Thermodynamic parameters obtained from the temperature-dependent UV-Vis experiments in toluene on the basis of the nucleation-elongation or isodesmic model.

	Conc. / M	Aggregation mode	α_{sat}	$\Delta H_e (\Delta H)^a$ / kJ/mol	$T_e (T_m)^b$ / K	K_a / M ⁻¹	$\langle N_n(T_e) \rangle$
Pd-1-LA⁷	1.0×10 ⁻⁵	Nucleation-elongation	1.153	-46.9	336.2	7.9×10 ⁻⁴	10.8
	2.5×10 ⁻⁵	Nucleation-elongation	1.081	-51.8	343.2	3.2×10 ⁻⁴	14.6
	5.0×10 ⁻⁵	Nucleation-elongation	1.016	-59.9	348.9	2.9×10 ⁻⁴	15.1
Pd/Pt (8/2)-1-LA	1.0×10 ⁻⁵	Nucleation-elongation	1.349	-30.0	334.7	9.4×10 ⁻⁴	10.2
Pd/Pt (5/5)-1-LA	1.0×10 ⁻⁵	Nucleation-elongation	1.452	-24.2	339.3	3.9×10 ⁻⁴	13.7
Pd/Pt (2/8)-1-LA	1.0×10 ⁻⁵	Nucleation-elongation	1.280	-30.7	339.2	4.2×10 ⁻³	6.2
Pt-1-LA	5.0×10 ⁻⁵	Nucleation-elongation	1.092	-36.2	362.4	3.2×10 ⁻⁵	31.5
Pd-2-LA	1.0×10 ⁻⁵	Isodesmic	--	-102.1	309.1	--	--
Pd/Pt (8/2)-2-LA	1.0×10 ⁻⁵	Isodesmic	--	-131.2	319.3	--	--
Pd/Pt (5/5)-2-LA	1.0×10 ⁻⁵	Isodesmic	--	-77.7	319.7	--	--
Pd/Pt (2/8)-2-LA	1.0×10 ⁻⁵	Isodesmic	--	-72.5	321.0	--	--
Pt-2-LA	1.0×10 ⁻⁵	Nucleation-elongation	1.450	-24.6	335.9	4.9×10 ⁻⁴	12.7
Pd-3-LA	5.0×10 ⁻⁵	Nucleation-elongation	1.025	-50.2	354.4	2.4×10 ⁻³	7.5
Pd/Pt (5/5)-3-LA	5.0×10 ⁻⁵	Nucleation-elongation	1.001	-63.5	362.0	-- ^c	-- ^c
Pt-3-LA	5.0×10 ⁻⁵	Nucleation-elongation	1.221	-24.0	363.0	-- ^c	-- ^c

^a ΔH_e for Nucleation-elongation and ΔH for isodesmic mode respectively. ^b T_e for Nucleation-elongation and T_m for isodesmic mode respectively. ^c Not determined due to the lack of data in the nucleation regime. ΔH_e : enthalpy corresponding to the aggregation (elongation) process; T_e : elongation temperature; α_{sat} : parameter introduced in the equation to ensure that $\alpha_{agg}/\alpha_{sat}$ does not exceed unity; K_a : dimensionless equilibrium constant of the activation step at the elongation temperature; $\langle N_n \rangle$: the number-averaged degree of polymerization in the elongation regime, averaged over all active species. T_m : the melting temperature in the isodesmic regime.

Supramolecular polymerization mechanism

The isodesmic self-association model assumes that monomers aggregate in an one dimensional, noncyclic manner.⁸⁻⁹ The reversible formation of noncovalent bonds is identical for all binding, in which the equilibrium constants and Gibbs free energy changes are equal for each step of the aggregation process. The cooperative nucleation-elongation model describes the equilibrium between the monomer pool and supramolecular polymers (oligomer nucleus formation), and the cooperative growth of the latter,⁹⁻¹² in which the process can be separated into a nucleation and an elongation phase.

The temperature-dependent isodesmic aggregation model can be described by the function as:

$$\alpha_{agg}(T) \approx \frac{1}{1 + \exp\left(-0.908\Delta H \frac{T - T_m}{RT_m^2}\right)} \quad (1)$$

Whereas, ΔH is enthalpy corresponding to the aggregation process and T_m is the melting temperature.

The temperature-dependent nucleation-elongation aggregation model can be described by the functions in two regimes:

Nucleation regime:

$$\alpha_{agg} = \sqrt[3]{K_a} \exp\left[\left(\frac{2}{3\sqrt[3]{K_a}} - 1\right) \frac{\Delta H_e}{RT_e^2} (T - T_e)\right] \quad (2)$$

Elongation regime:

$$\alpha_{agg} = \alpha_{sat} \left(1 - \exp\left[\frac{-\Delta H_e}{RT_e^2} (T - T_e)\right]\right) \quad (3)$$

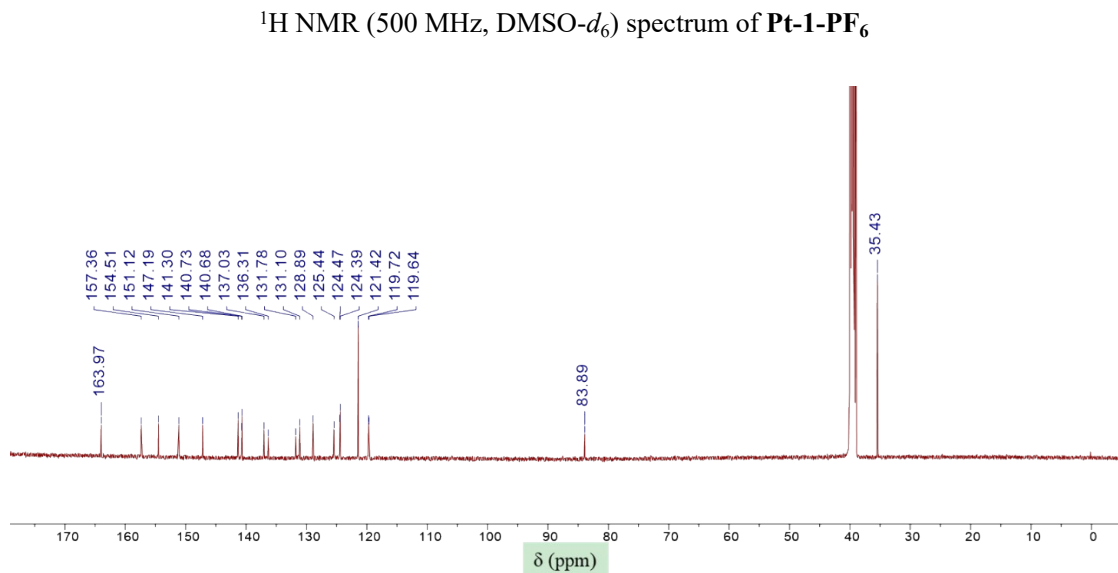
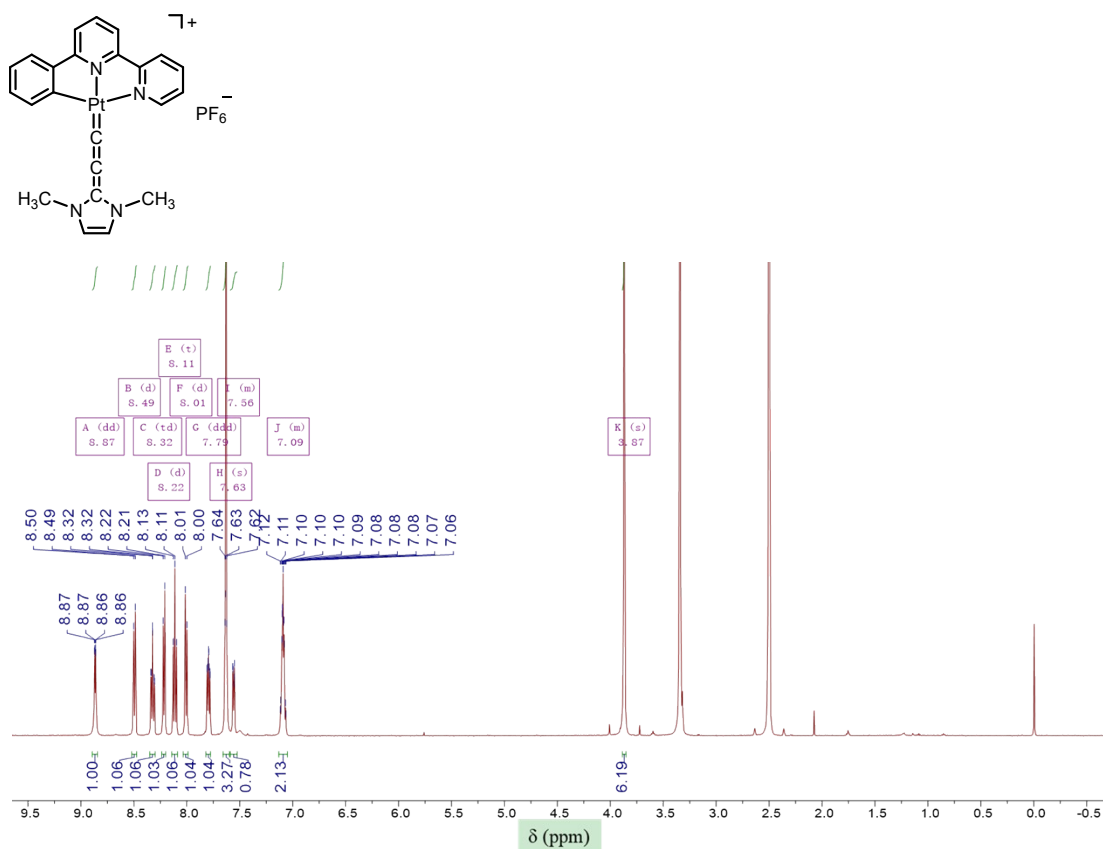
$$\langle N_n \rangle = \frac{1}{\sqrt{K_a}} \sqrt{\frac{\alpha_{agg}}{\alpha_{sat} - \alpha_{agg}}} \quad (4)$$

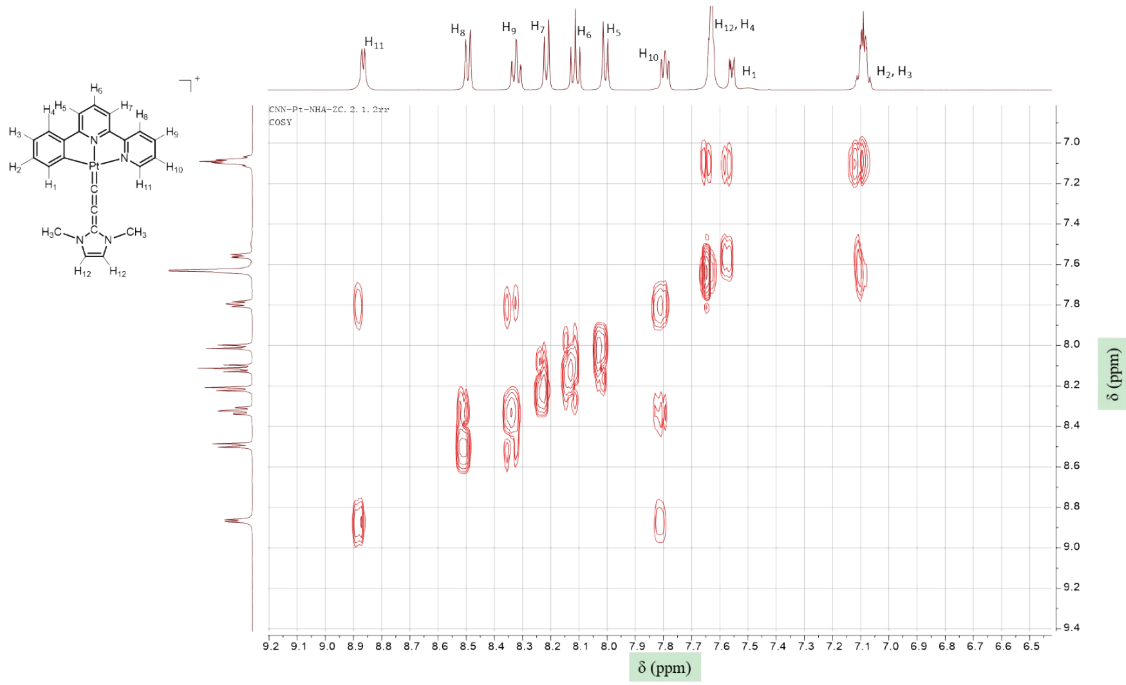
$$\langle N_n(T_e) \rangle = \frac{1}{\sqrt[3]{K_a}} \quad (5)$$

Whereas, ΔH_e is enthalpy corresponding to the aggregation (elongation) process; T_e is elongation temperature; α_{sat} is parameter introduced in the equation to ensure that $\alpha_{agg}/\alpha_{sat}$ does not exceed unity; K_a is dimensionless equilibrium constant of the activation step at the elongation temperature; $\langle N_n \rangle$ is the number-averaged degree of polymerization in the elongation regime, averaged over all

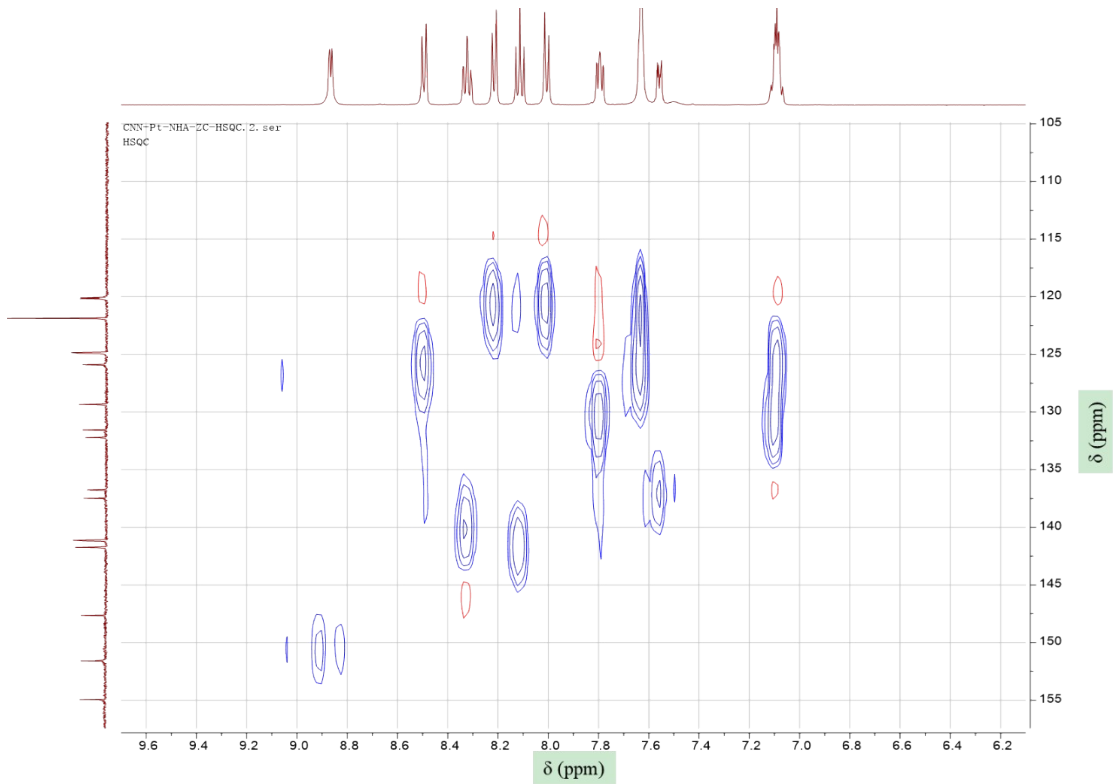
active species.

NMR spectra

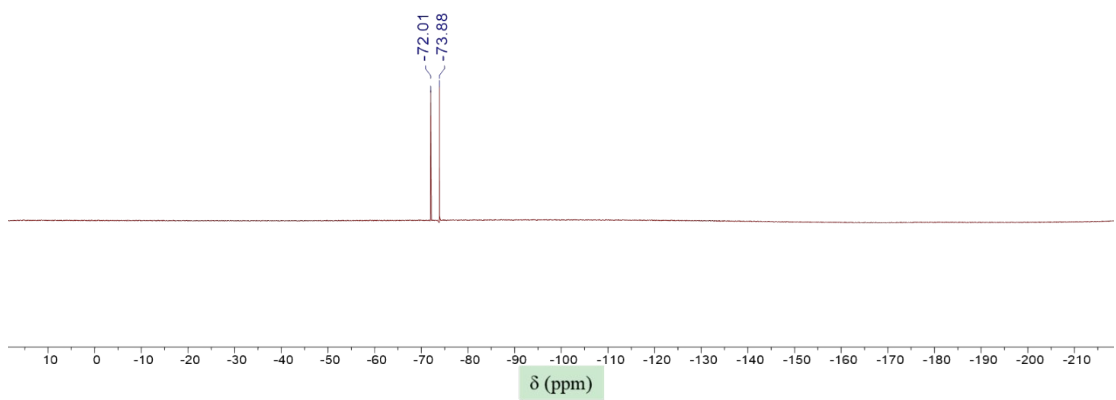




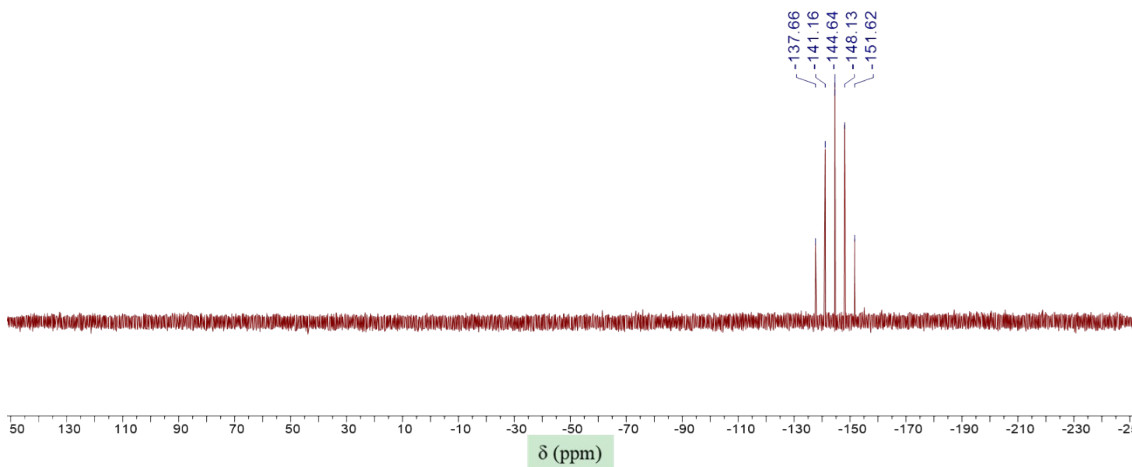
^1H - ^1H COSY (DMSO-*d*₆) spectrum of **Pt-1-PF**₆



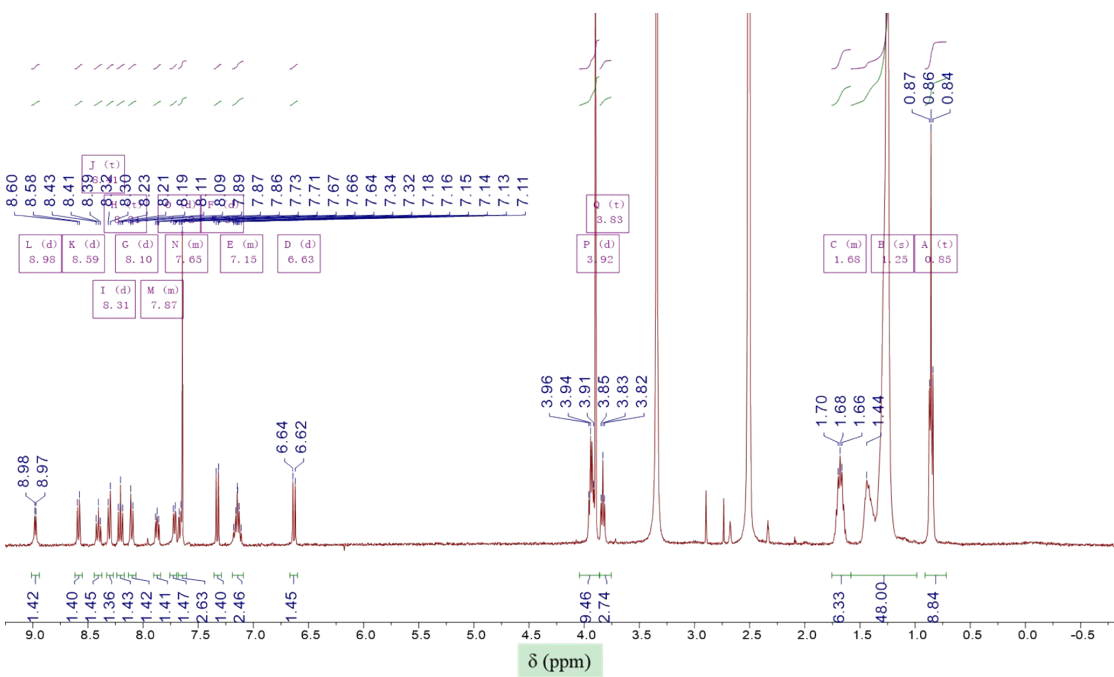
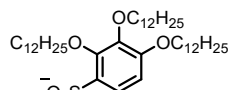
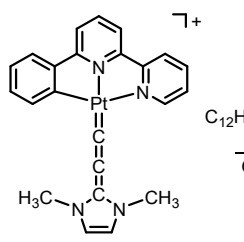
C-H COSY (HSQC, DMSO-*d*₆) spectrum of **Pt-1-PF**₆



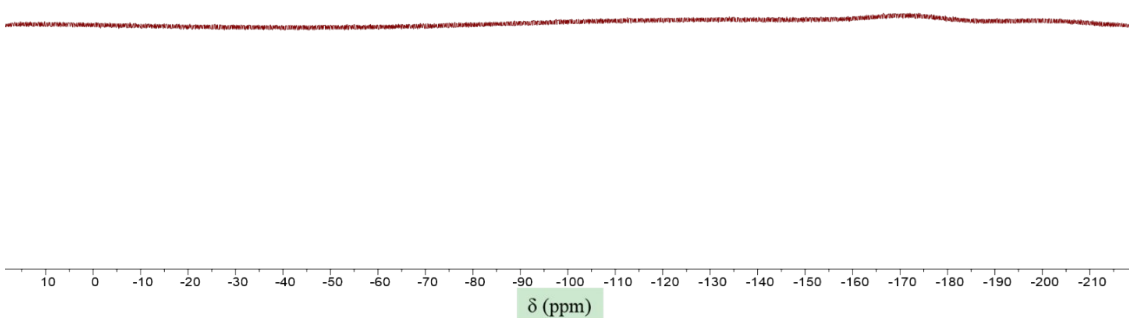
^{19}F NMR (376 MHz, MeCN- d_3) spectrum of **Pt-1-PF₆**



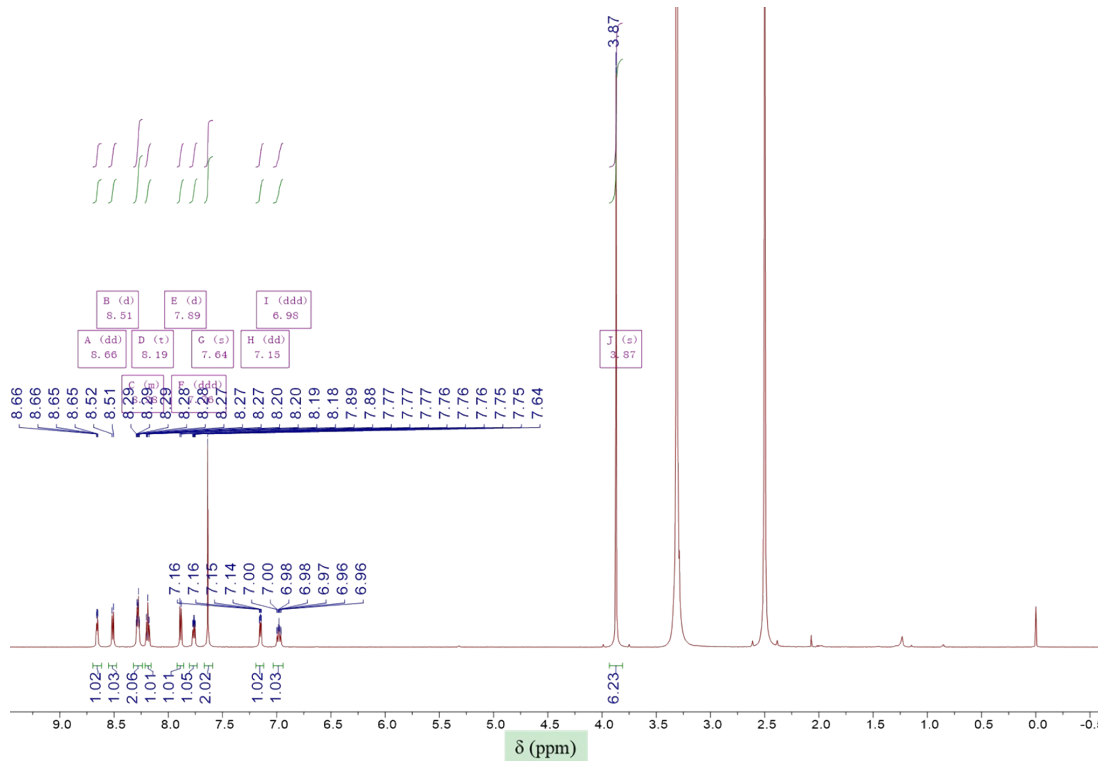
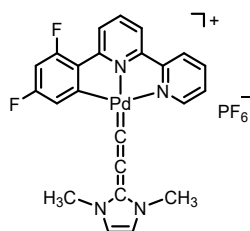
^{31}P NMR (202 MHz, MeCN- d_3) spectrum of **Pt-1-PF₆**



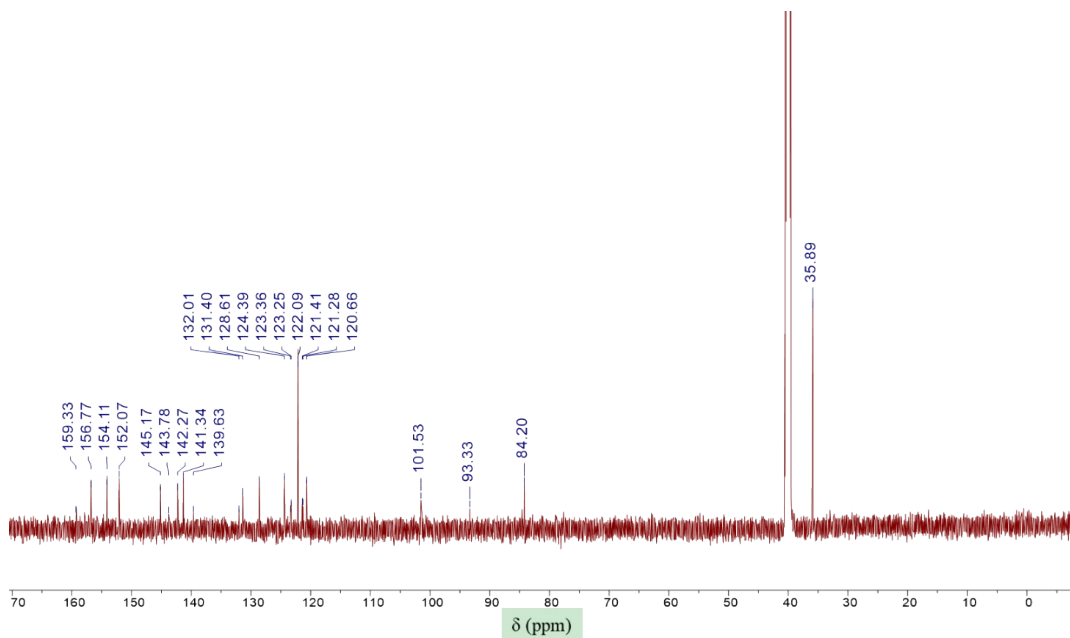
¹H NMR (400 MHz, DMSO-*d*₆) spectrum of **Pt-1-LA**



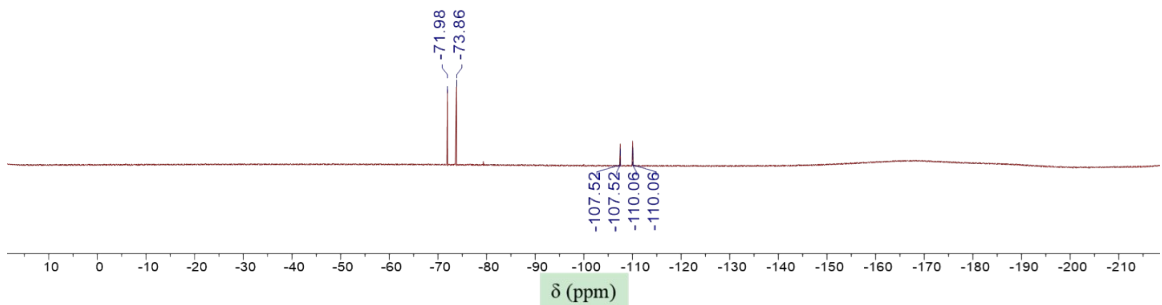
¹⁹F NMR (376 MHz, DMSO-*d*₆) spectrum of **Pt-1-LA**



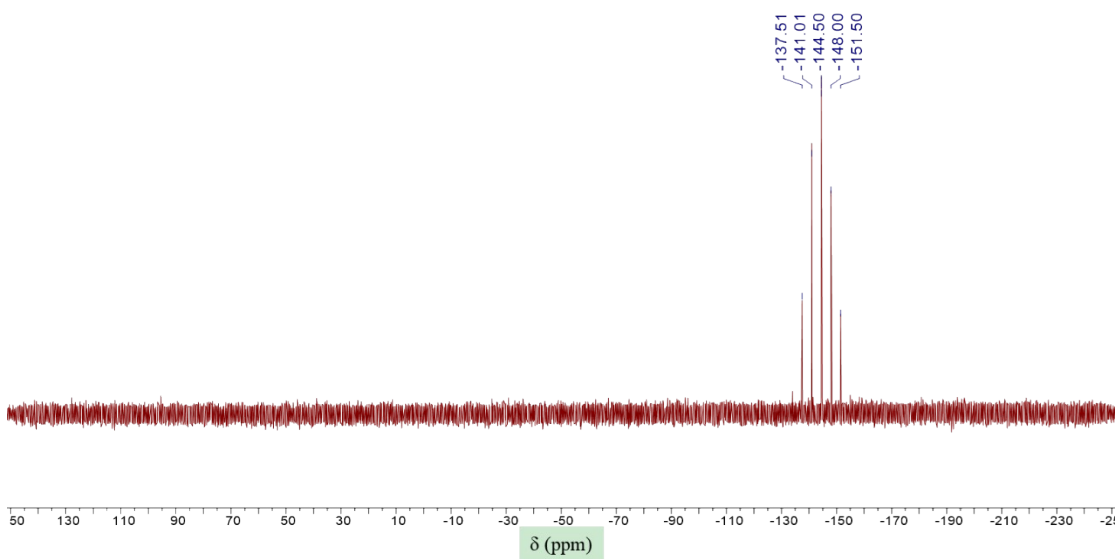
^1H NMR (600 MHz, $\text{DMSO}-d_6$) spectrum of **Pd-2-PF₆**



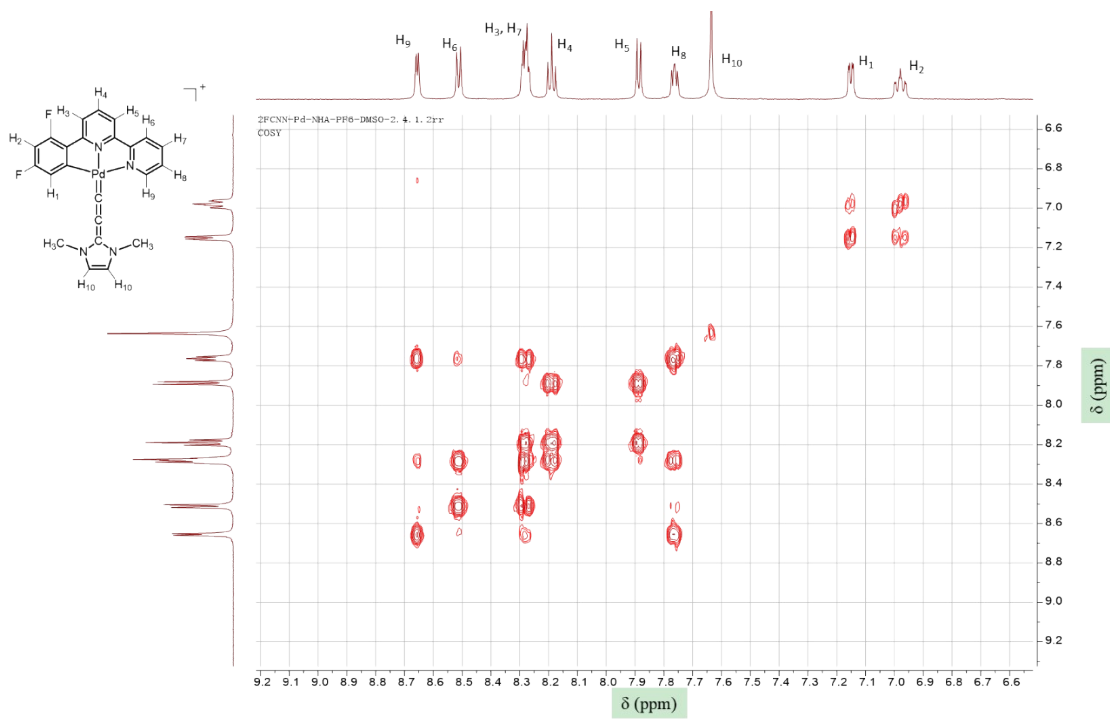
^{13}C NMR (151 MHz, $\text{DMSO}-d_6$) spectrum of **Pd-2-PF₆**



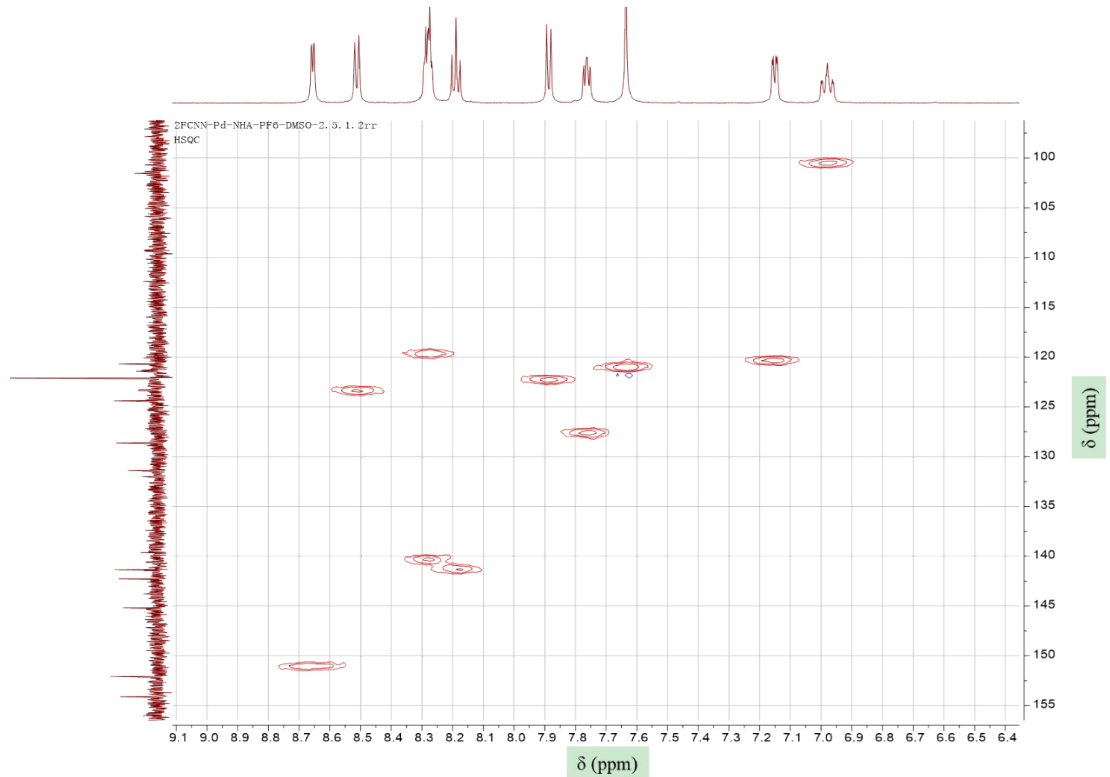
^{19}F NMR (376 MHz, MeCN- d_3) spectrum of **Pd-2-PF**₆



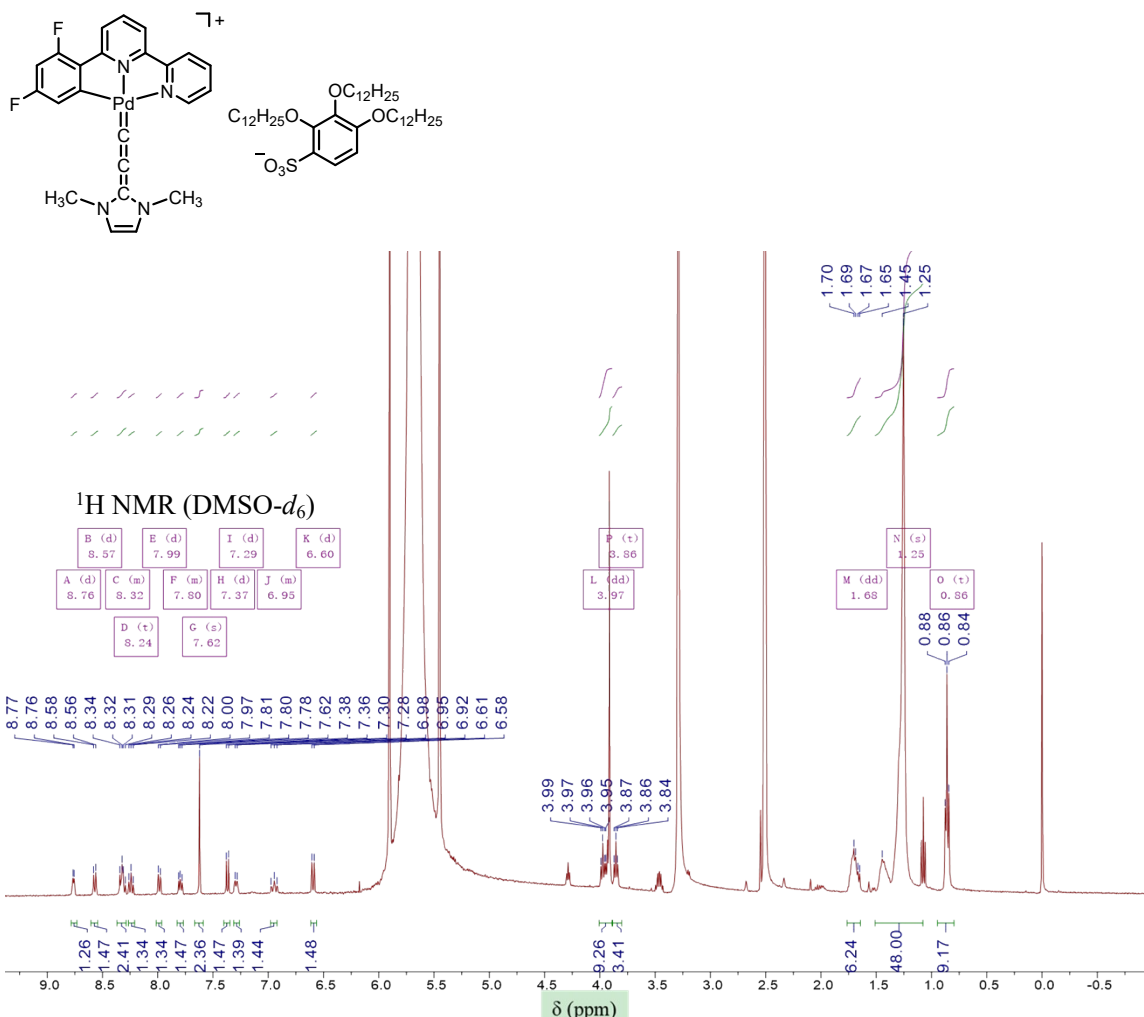
^{31}P NMR (202 MHz, MeCN- d_3) spectrum of **Pd-2-PF**₆



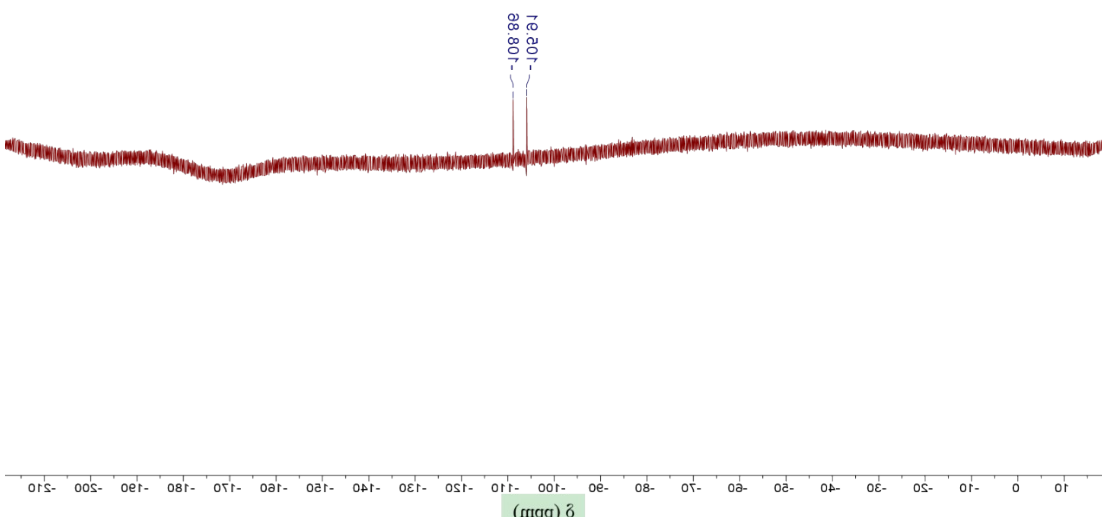
¹H-¹H COSY (DMSO-*d*₆) spectrum of **Pd-2-PF₆**



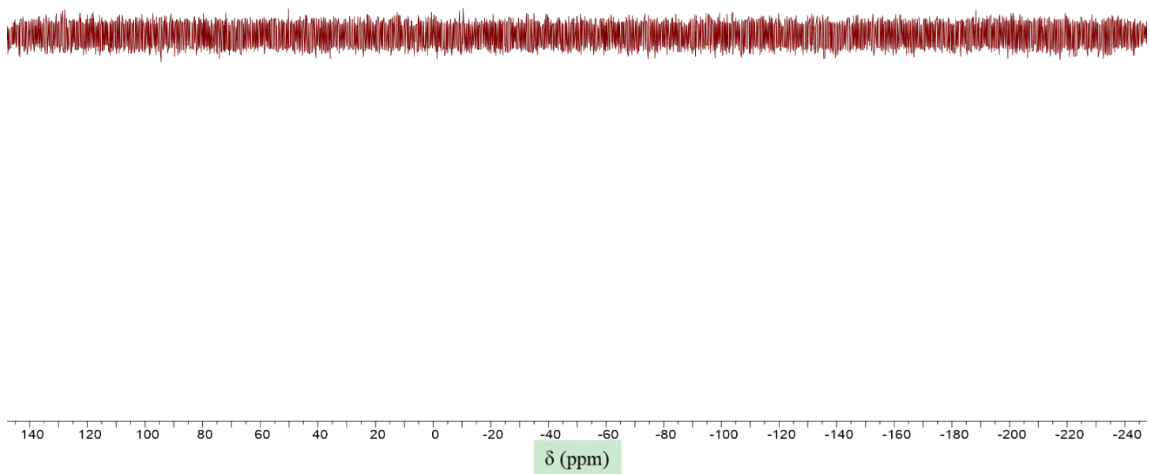
C-H COSY (HSQC, DMSO-*d*₆) spectrum of **Pd-2-PF₆**



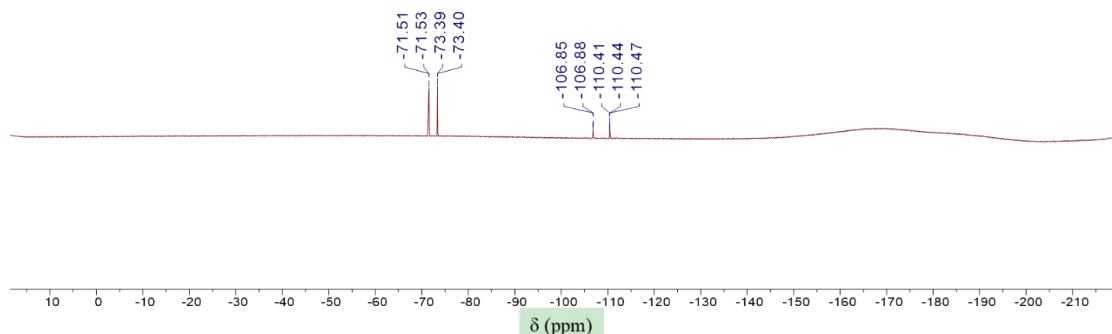
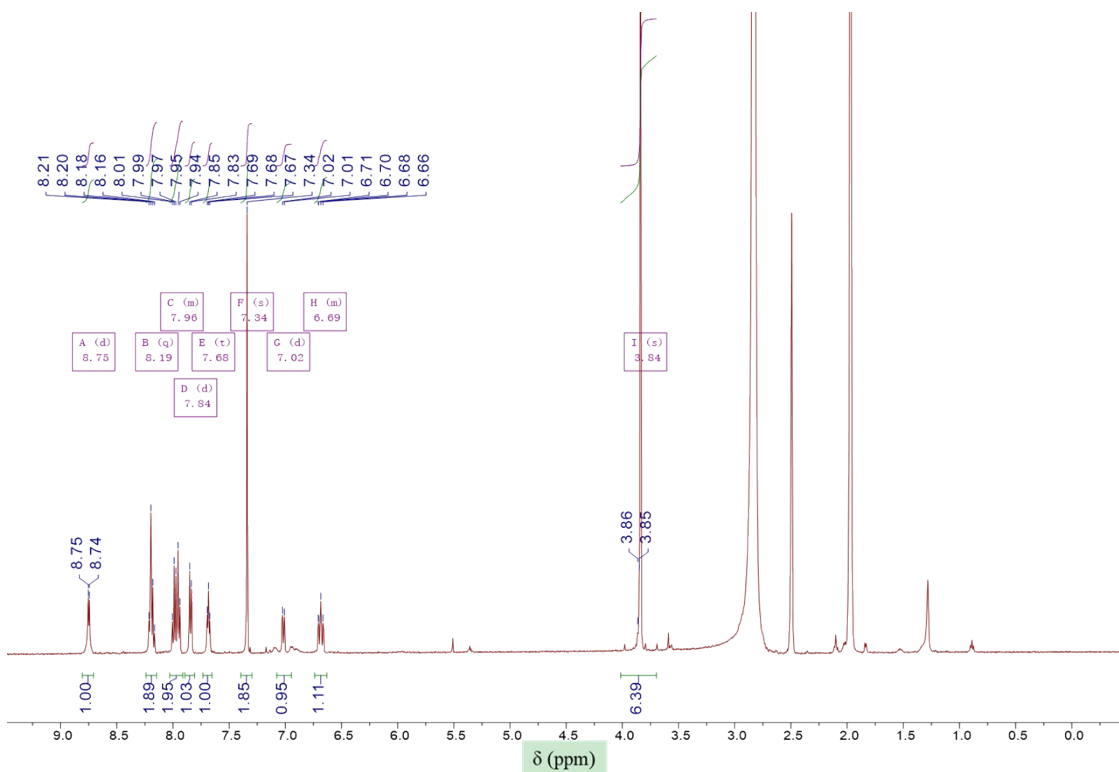
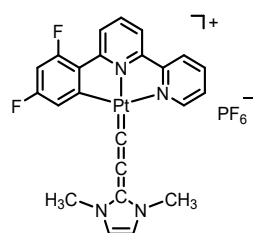
¹H NMR (400 MHz, DMSO-*d*₆+ minor CD₂Cl₂) spectrum of **Pd-2-LA**

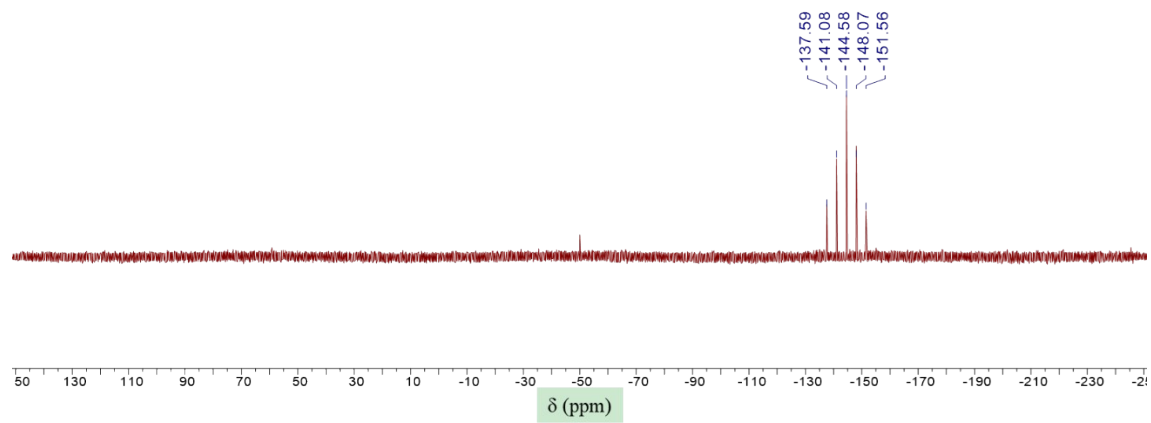


¹⁹F NMR (376 MHz, DMSO-*d*₆ + minor CD₂Cl₂) spectrum of **Pd-2-LA**

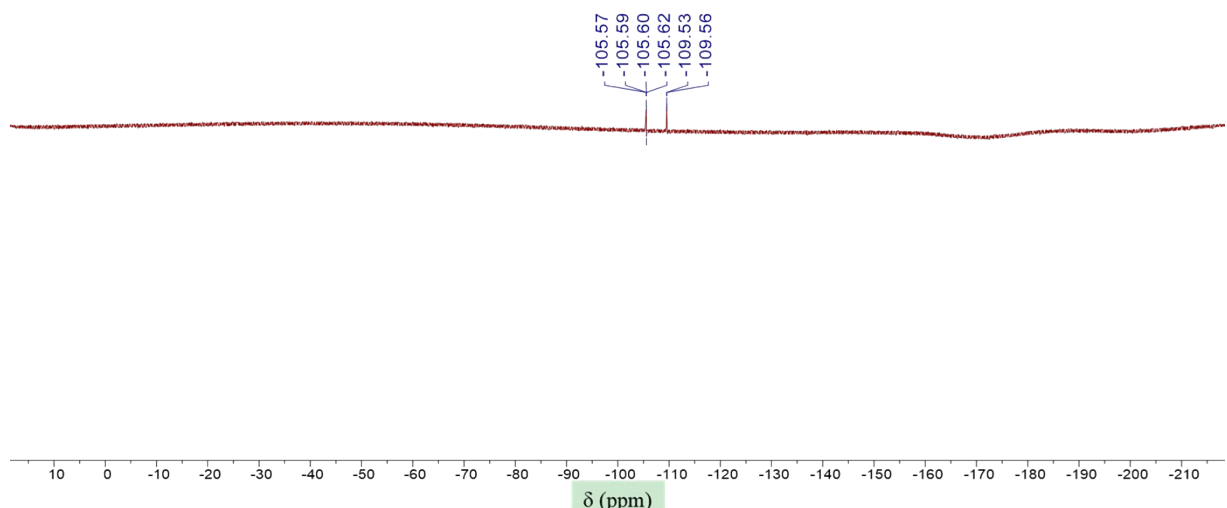
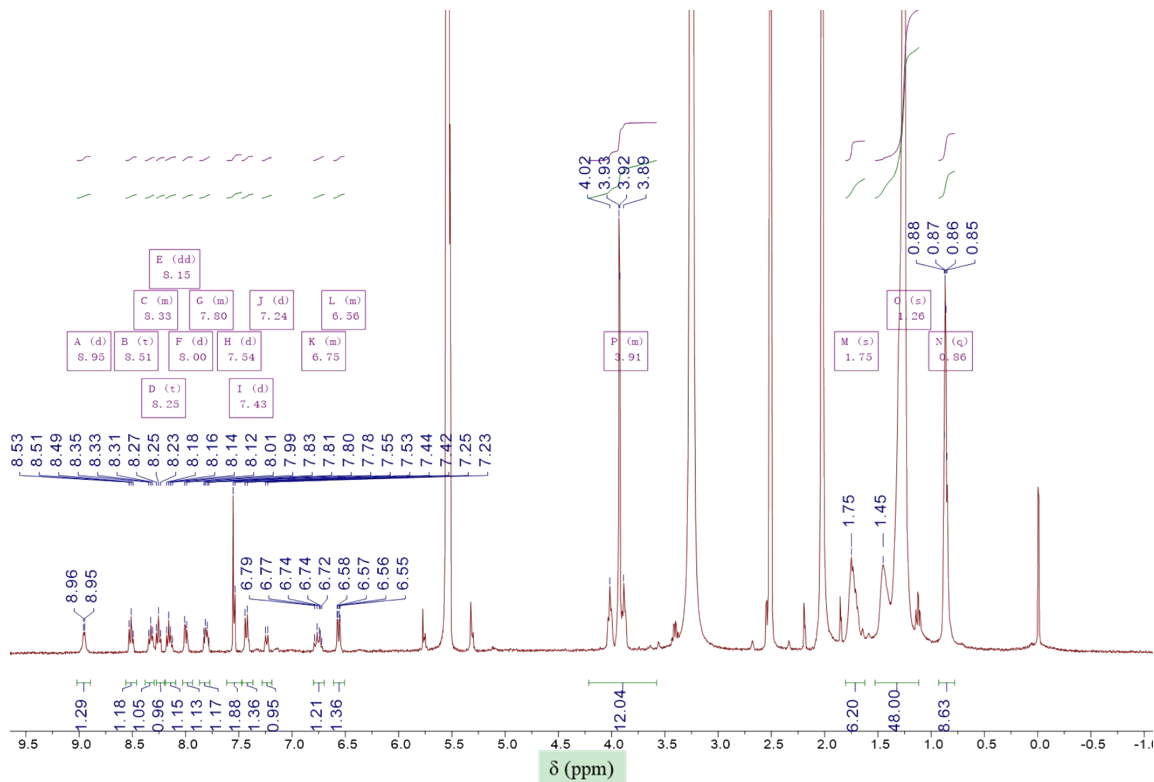
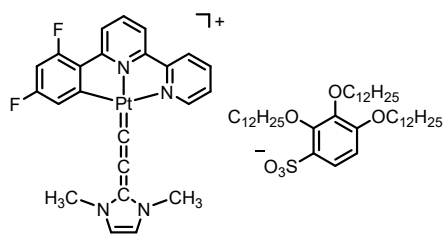


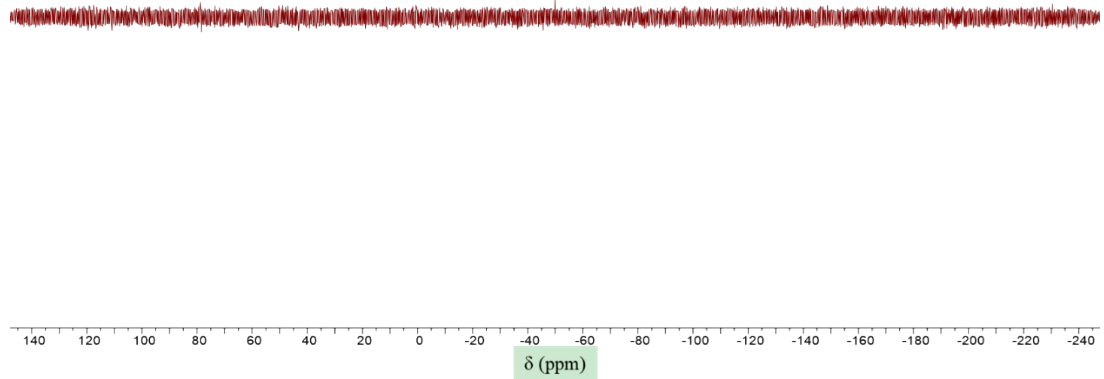
^{31}P NMR (202 MHz, DMSO- d_6 + minor CD₂Cl₂) spectrum of **Pd-2-LA**



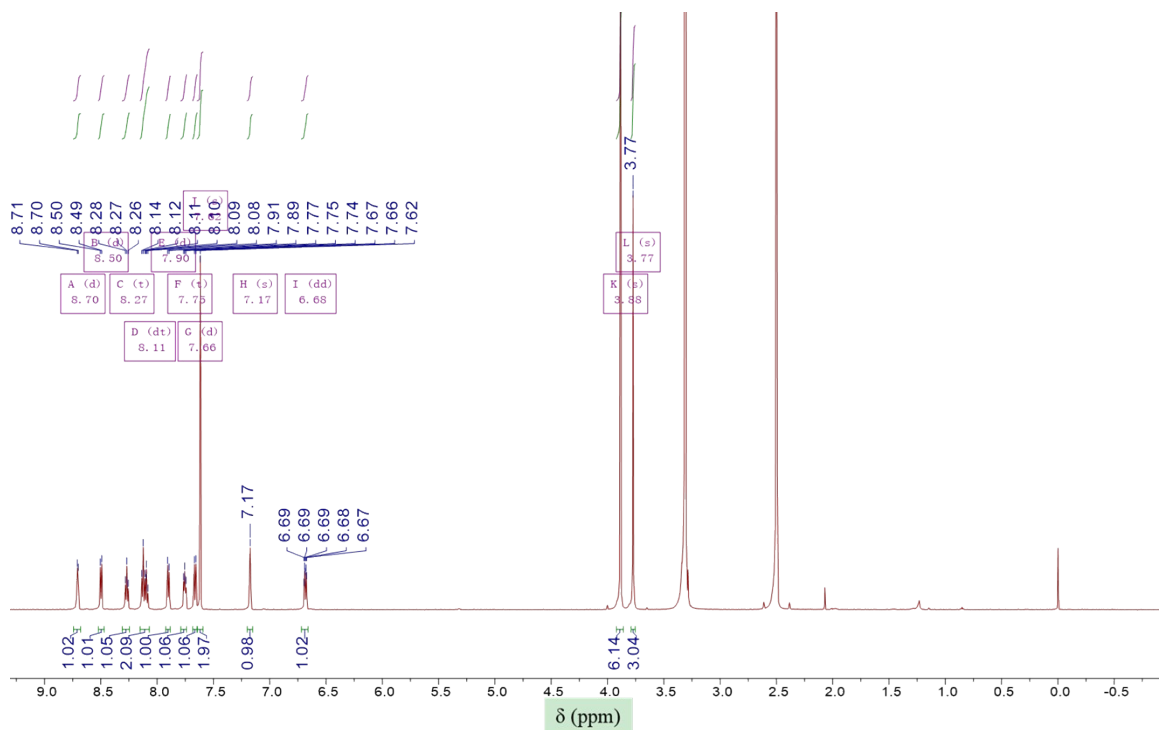
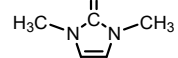
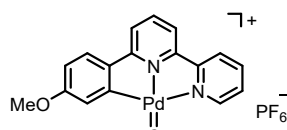


^{31}P NMR (202 MHz, MeCN- d_3) spectrum of **Pt-2-PF₆**

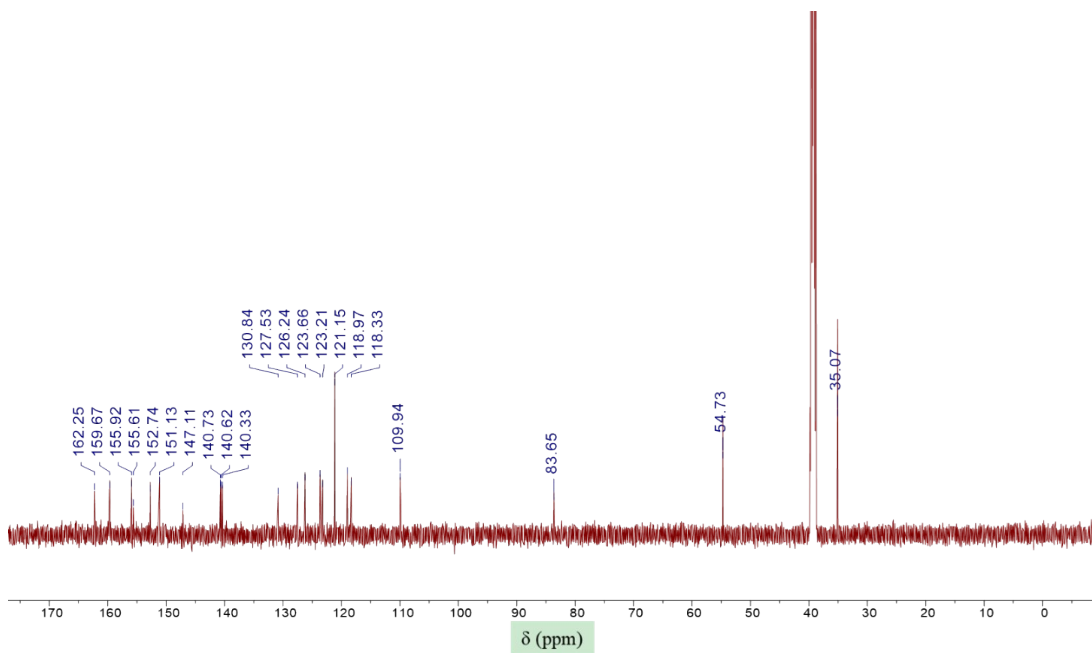




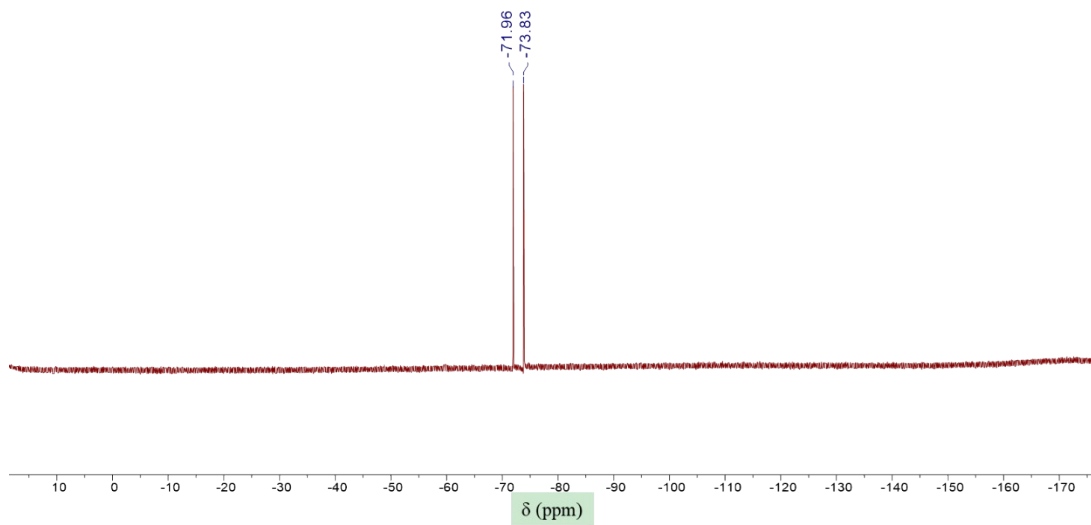
^{31}P NMR (202 MHz, DMSO- d_6 + minor CD₂Cl₂) spectrum of **Pt-2-LA**



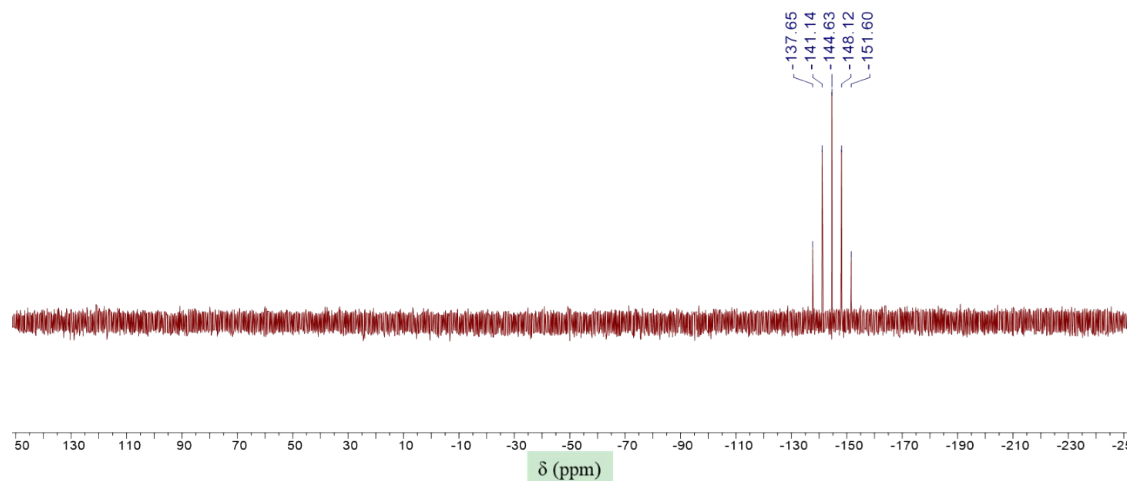
¹H NMR (600 MHz, DMSO-*d*₆) spectrum of **Pd-3-PF₆**



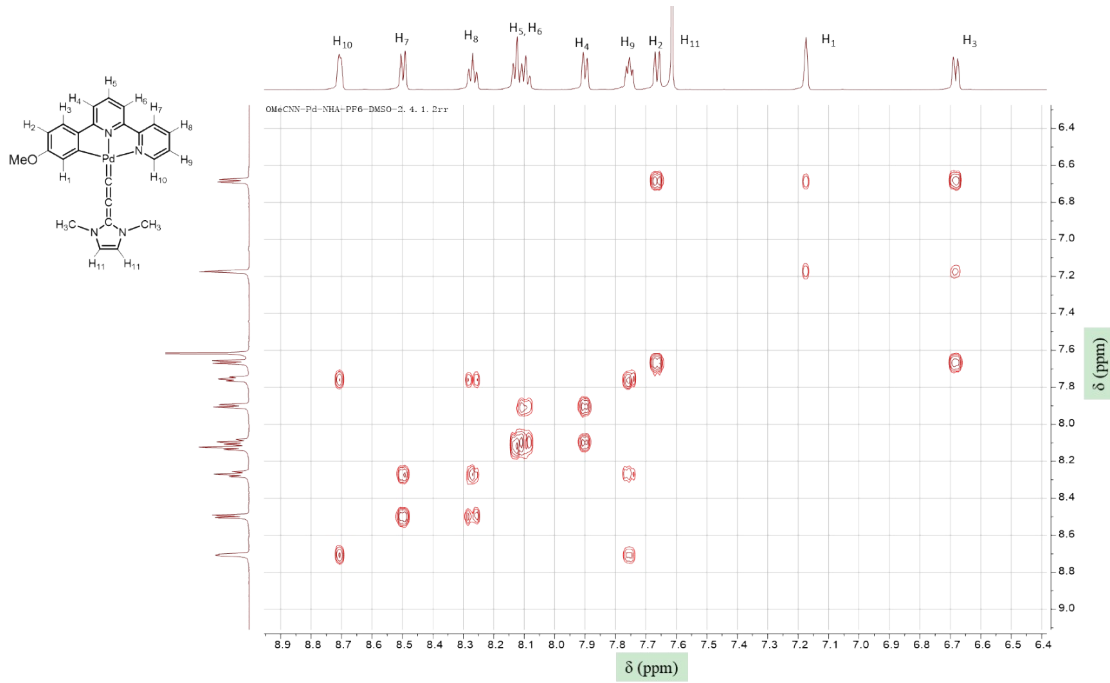
¹³C NMR (151 MHz, DMSO-*d*₆) spectrum of **Pd-3-PF₆**



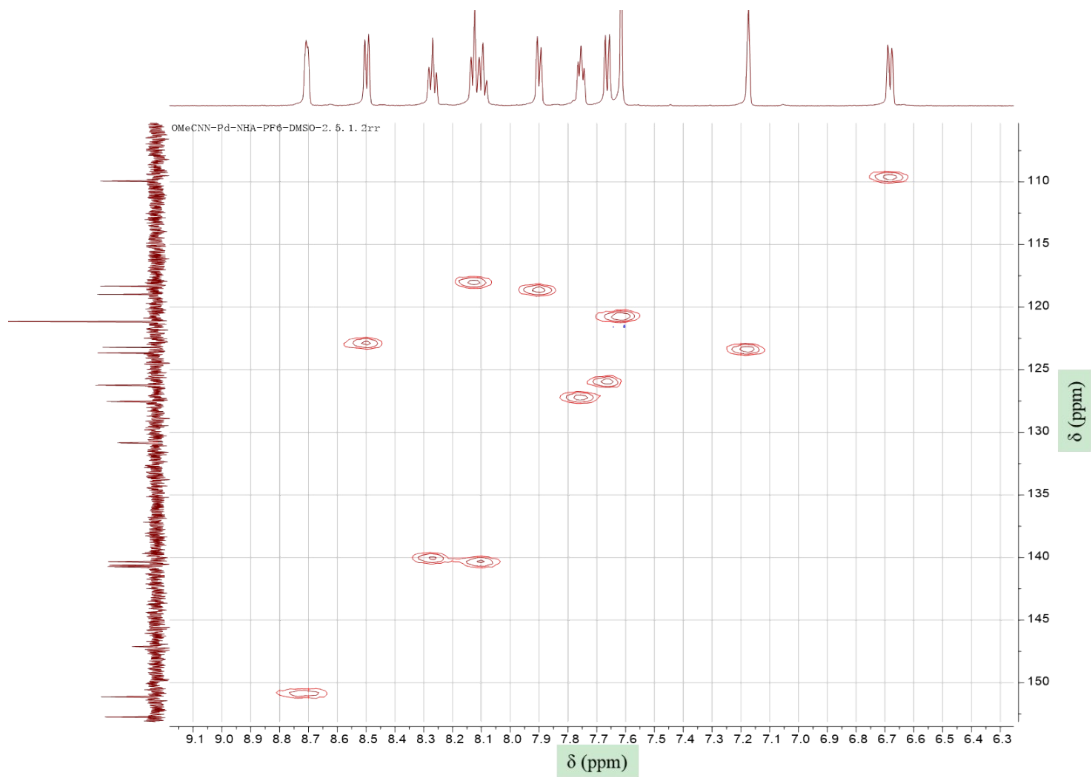
^{19}F NMR (376 MHz, MeCN- d_3) spectrum of **Pd-3-PF₆**



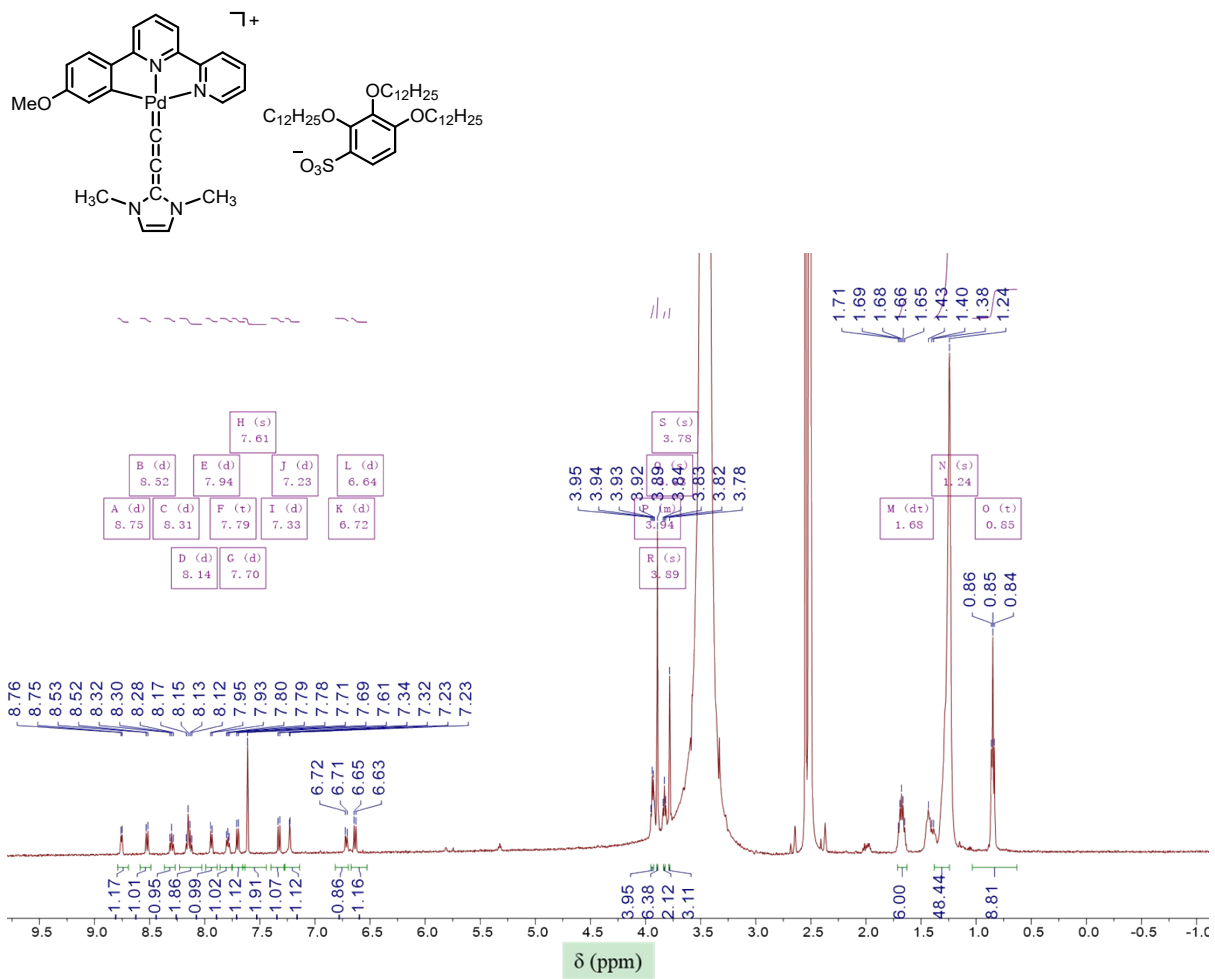
^{31}P NMR (202 MHz, MeCN- d_3) spectrum of **Pd-3-PF₆**



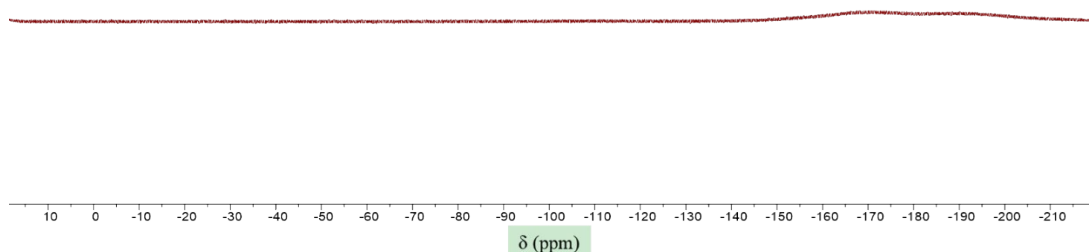
¹H-¹H COSY (DMSO-*d*₆) spectrum of **Pd-3-PF₆**



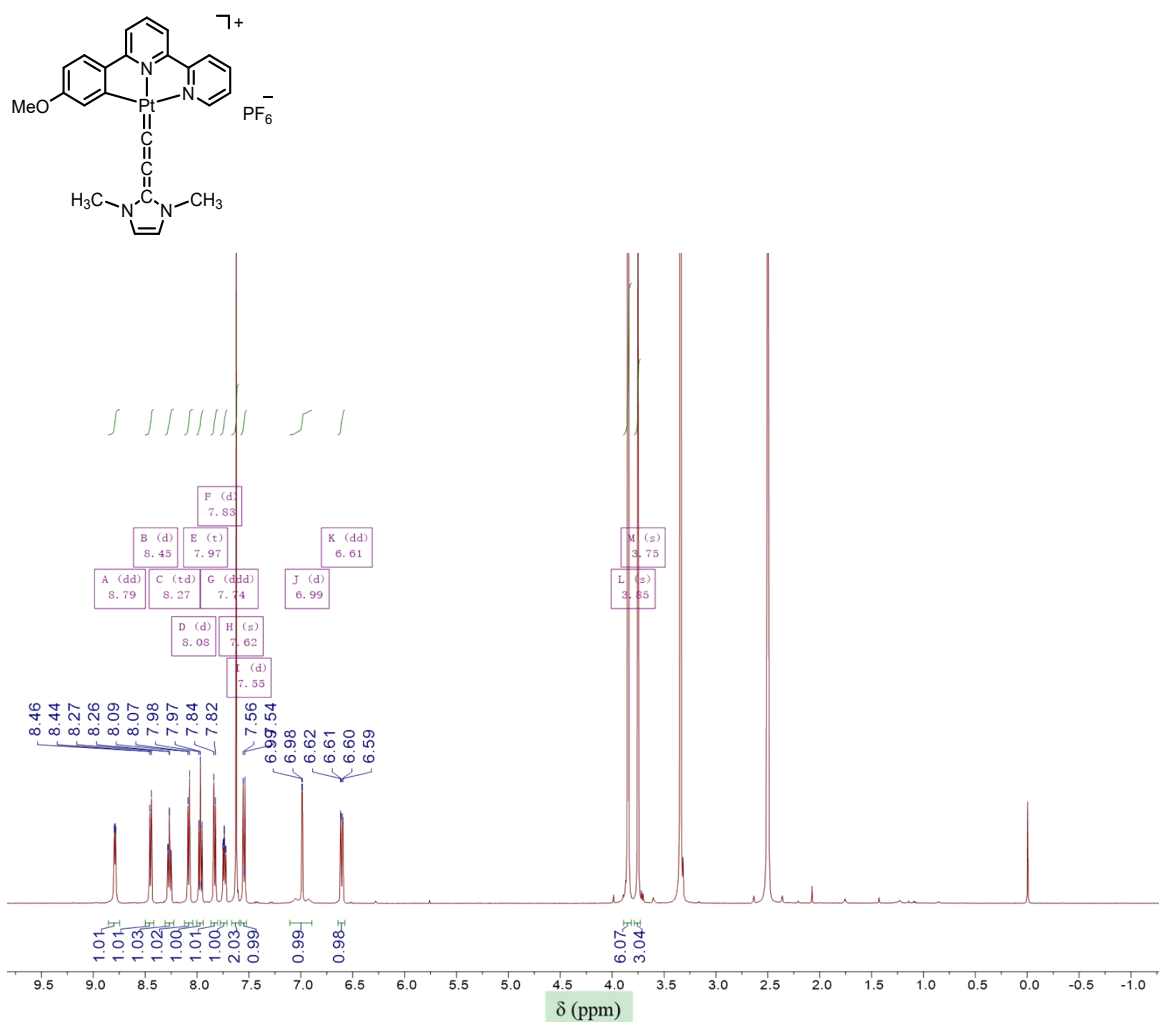
C-H COSY (HSQC, DMSO-*d*₆) spectrum of **Pd-3-PF₆**



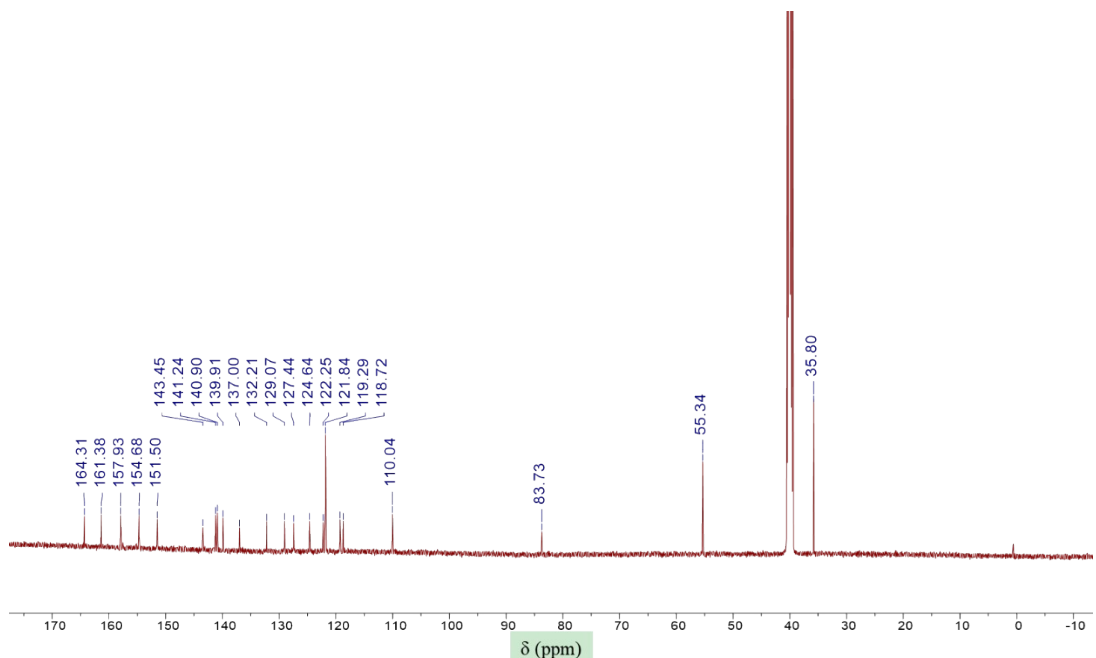
¹H NMR (500 MHz, DMSO-*d*₆) spectrum of Pd-3-LA

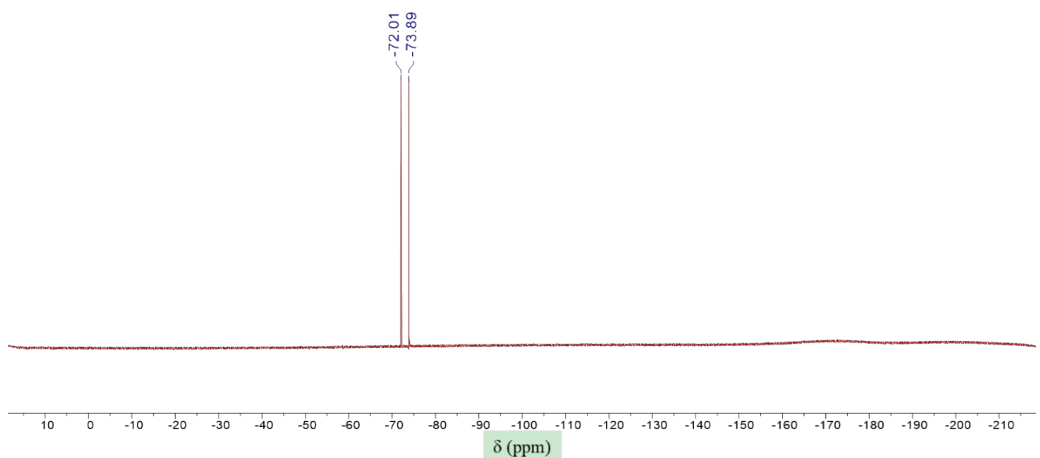


¹⁹F NMR (376 MHz, DMSO-*d*₆) spectrum of Pd-3-LA

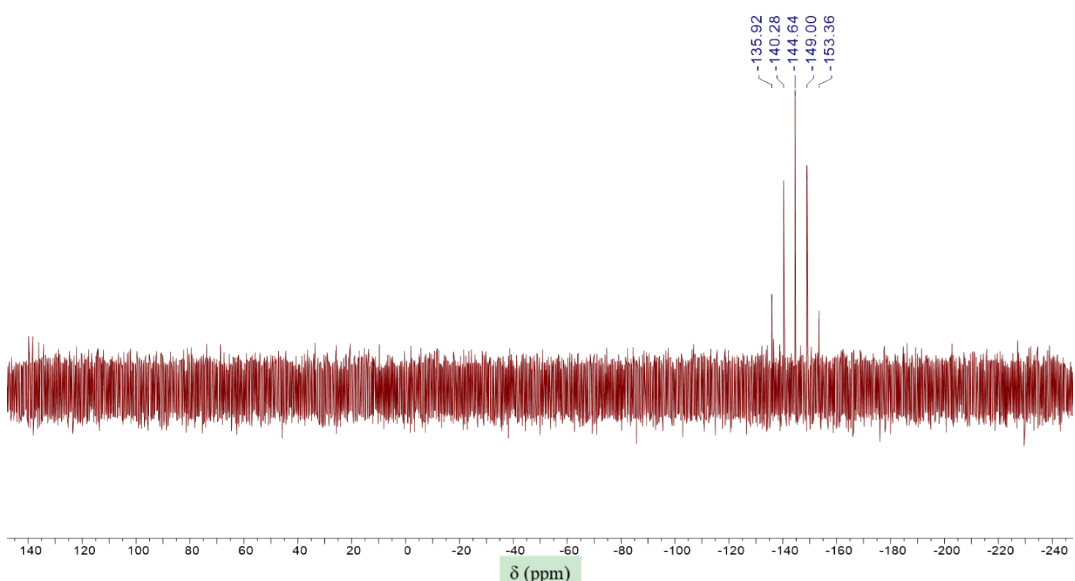


¹H NMR (500 MHz, DMSO-*d*₆) spectrum of Pt-3-PF₆

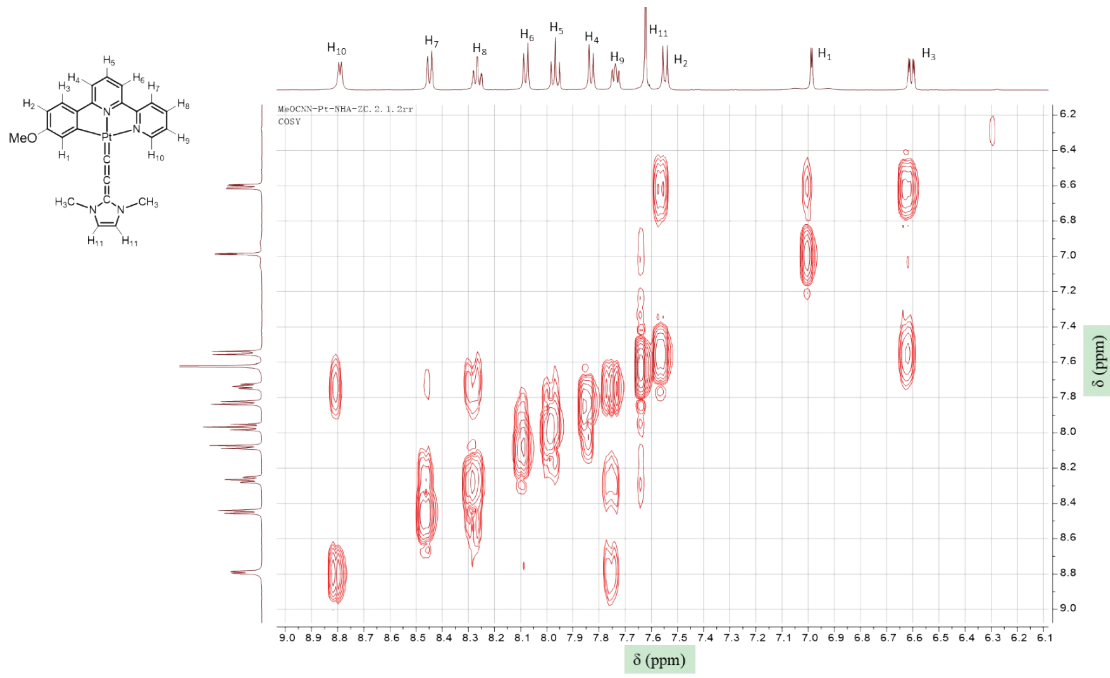




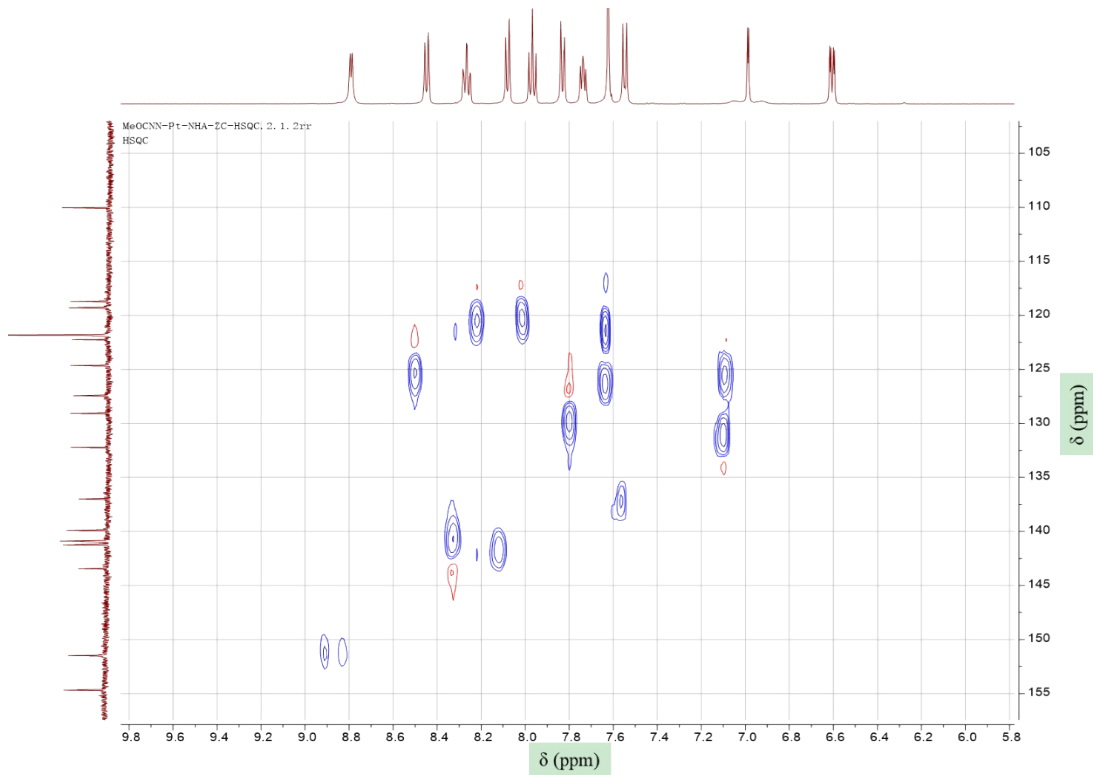
^{19}F NMR (376 MHz, MeCN- d_3) spectrum of **Pt-3-PF₆**



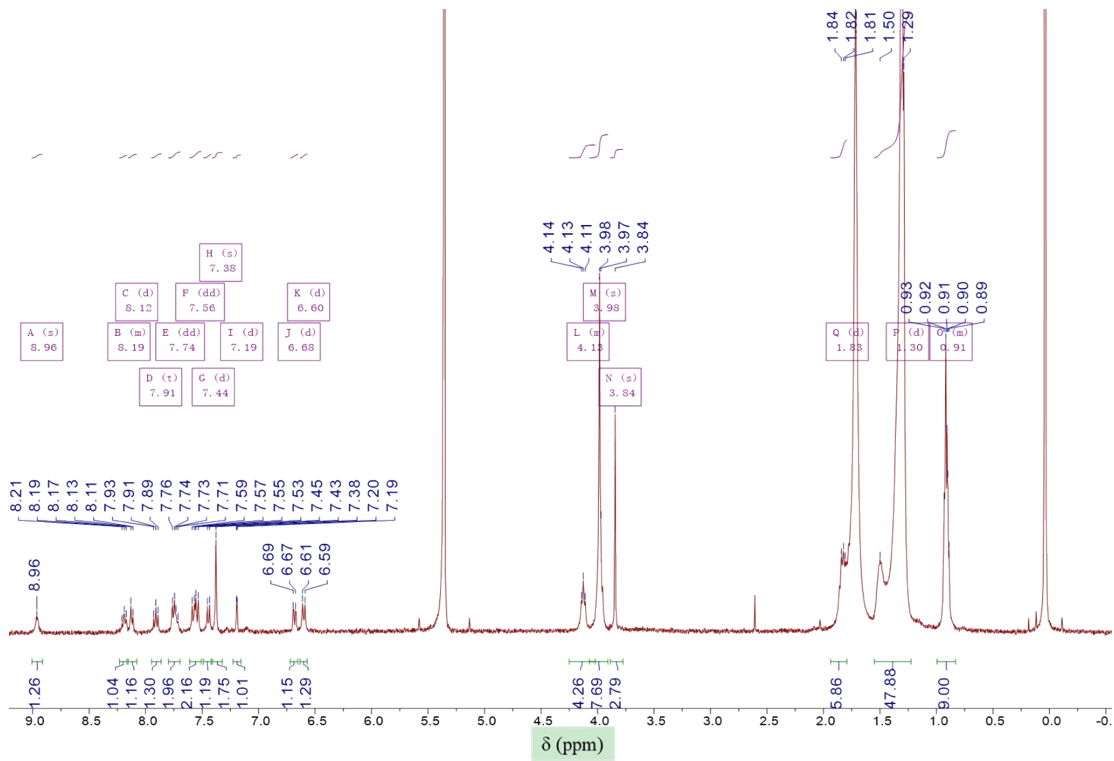
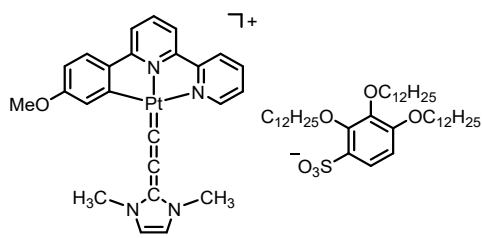
^{31}P NMR (162 MHz, MeCN- d_3) spectrum of **Pt-3-PF₆**



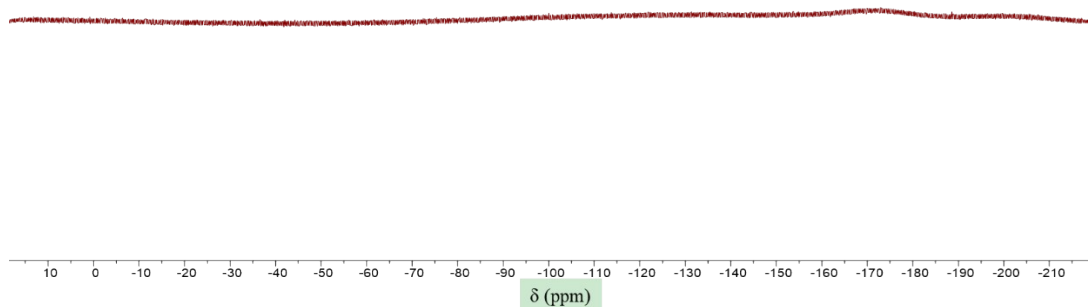
^1H - ^1H COSY (DMSO-*d*₆) spectrum of **Pt-3-PF**₆



C-H COSY (HSQC, DMSO-*d*₆) spectrum of **Pt-3-PF**₆

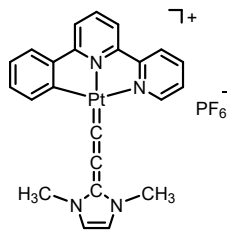


¹H NMR (400 MHz, CD₂Cl₂) spectrum of Pt-3-LA

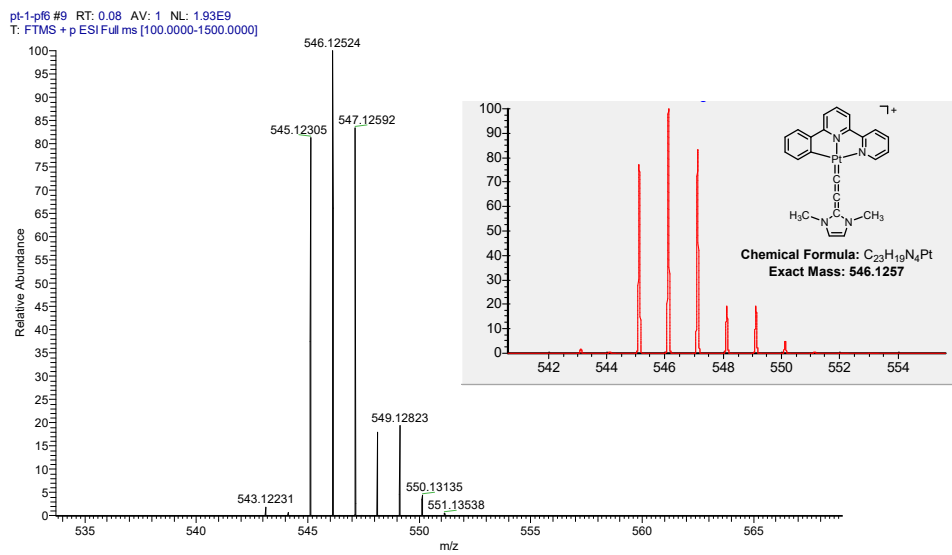


¹⁹F NMR (376 MHz, DMSO-*d*₆) spectrum of Pt-3-LA

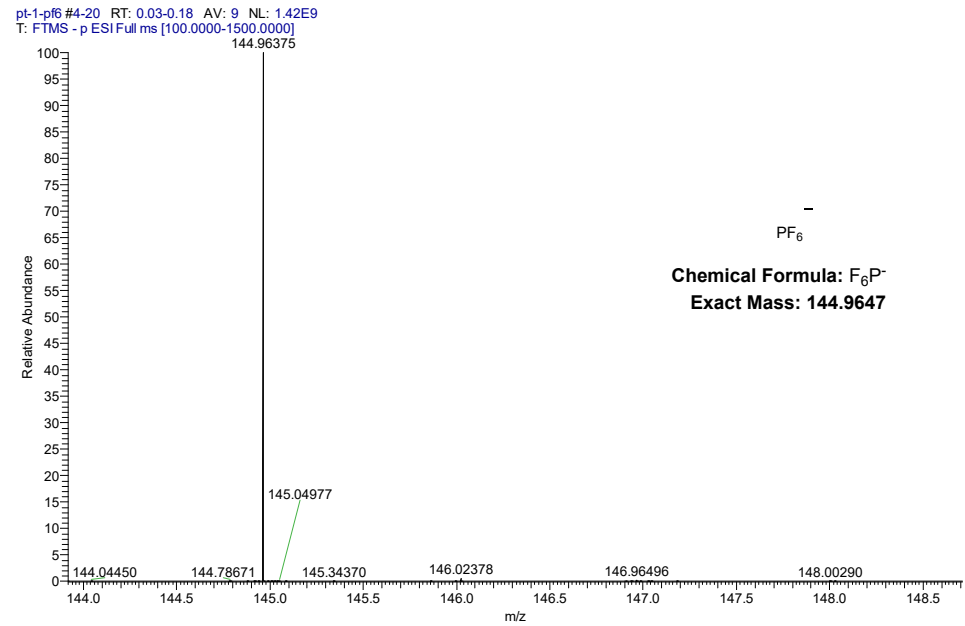
High Resolution Mass Spectra

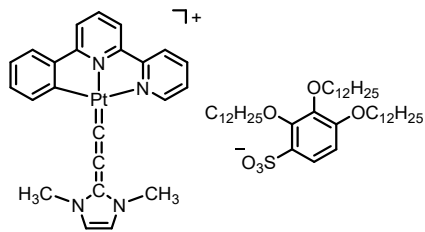


Positive mode:

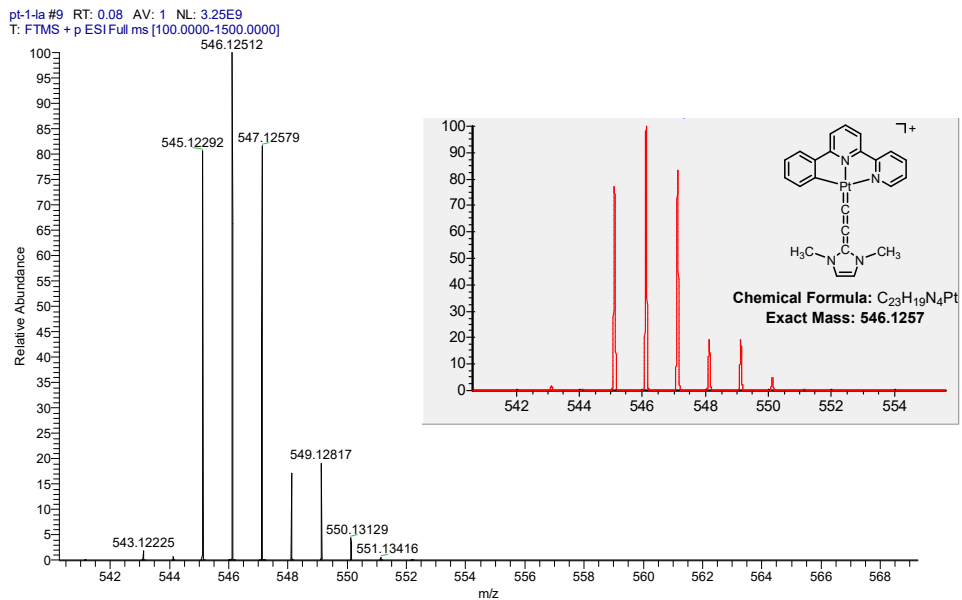


Negative mode:

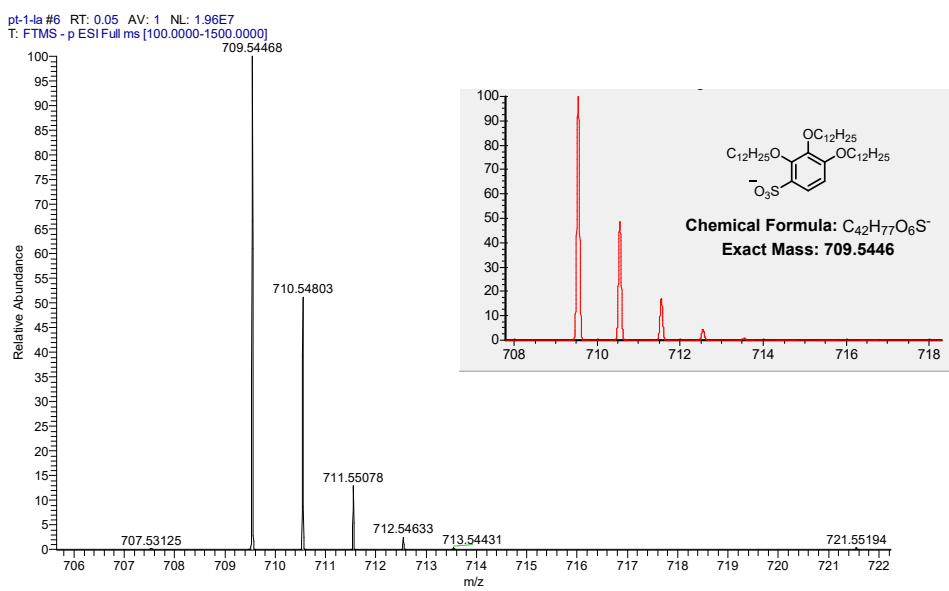


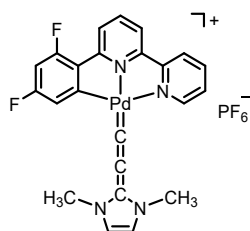


Positive mode:

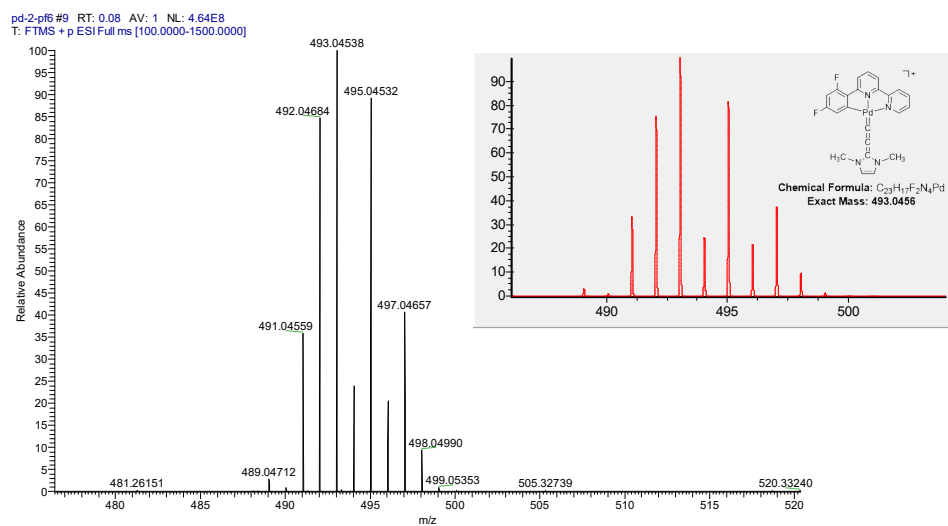


Negative mode:

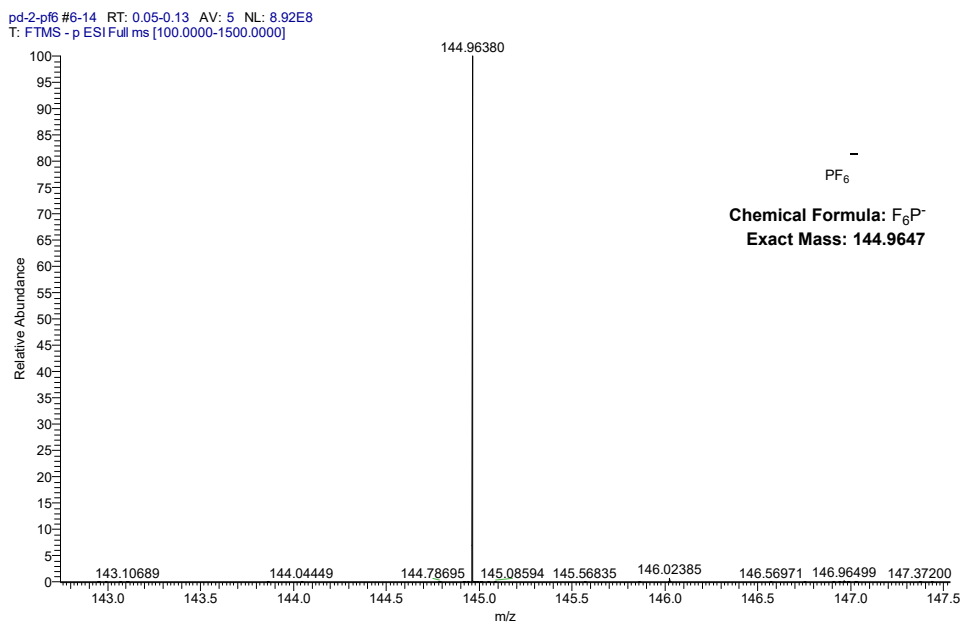


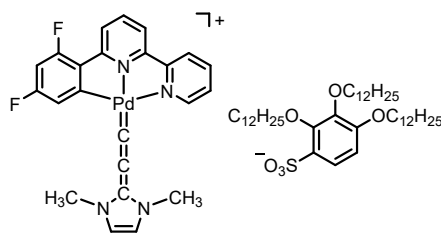


Positive mode:

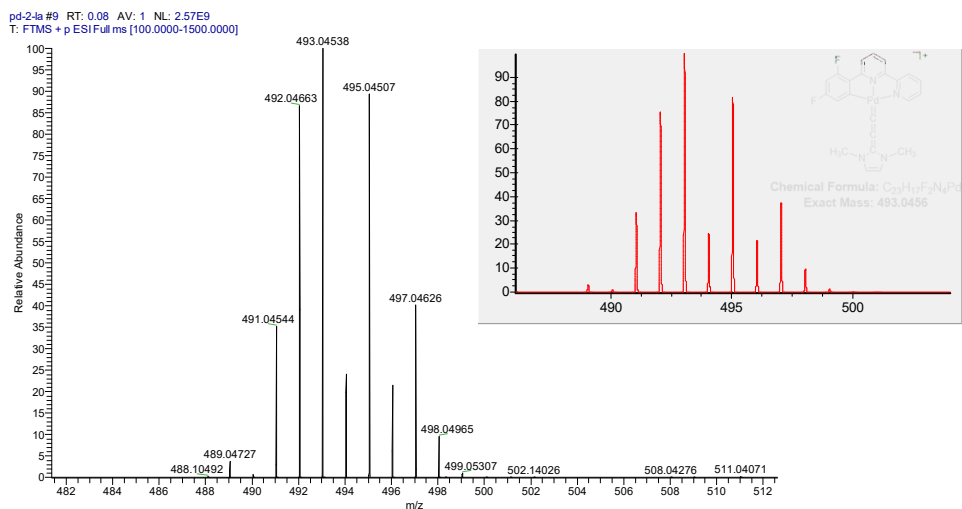


Negative mode:

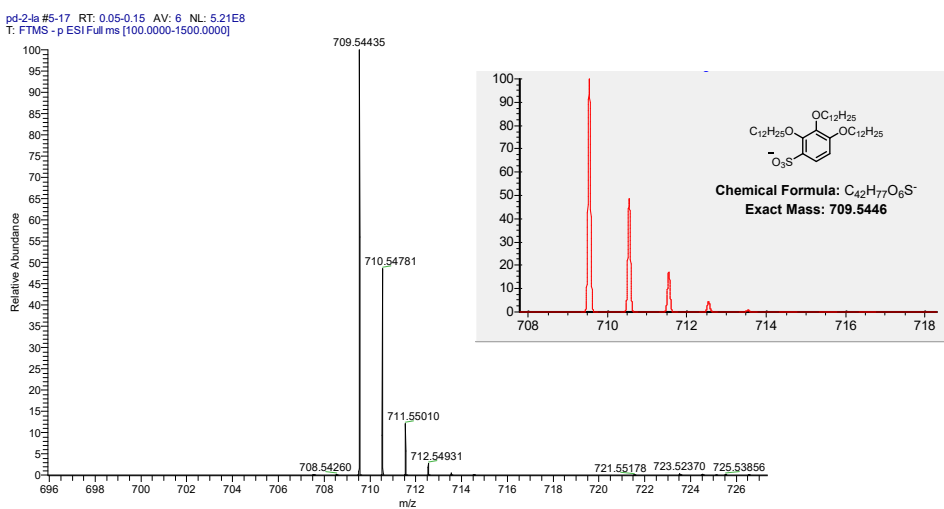


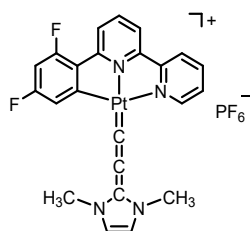


Positive mode:

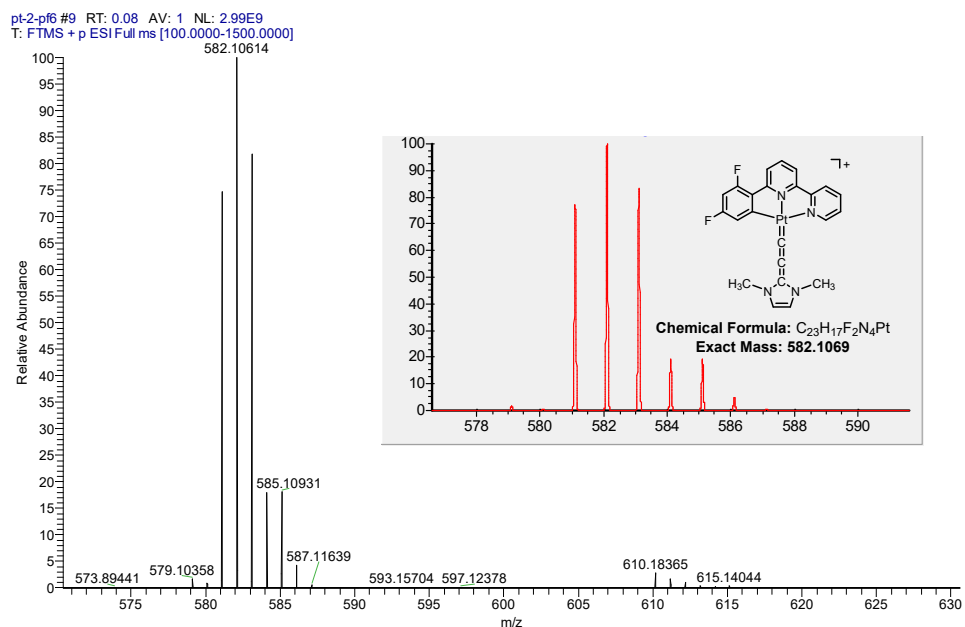


Negative mode:

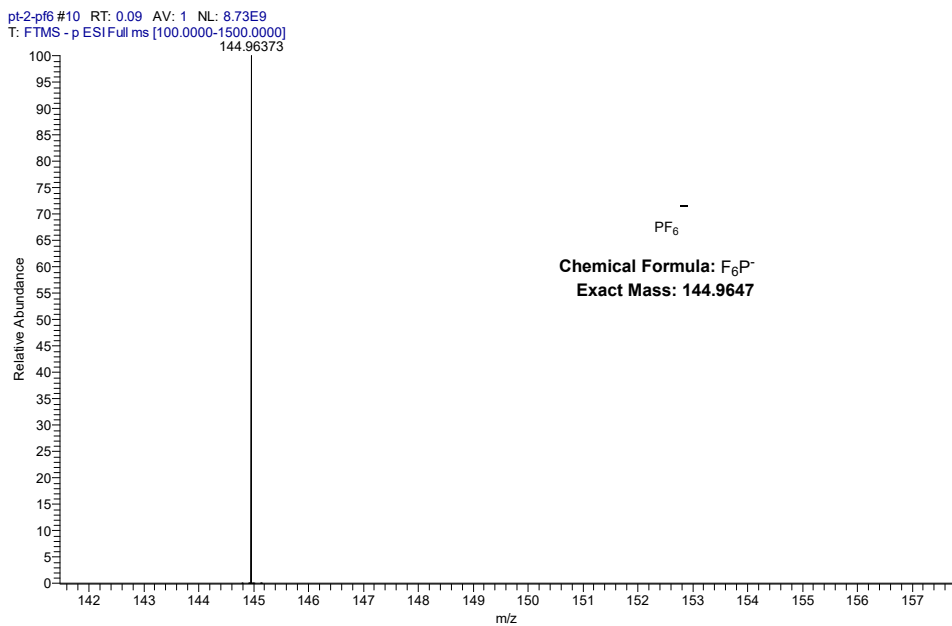


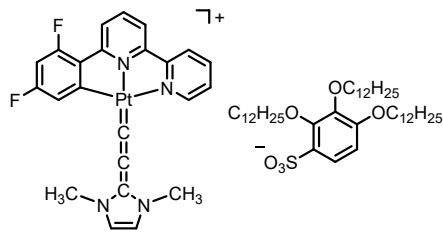


Positive mode:

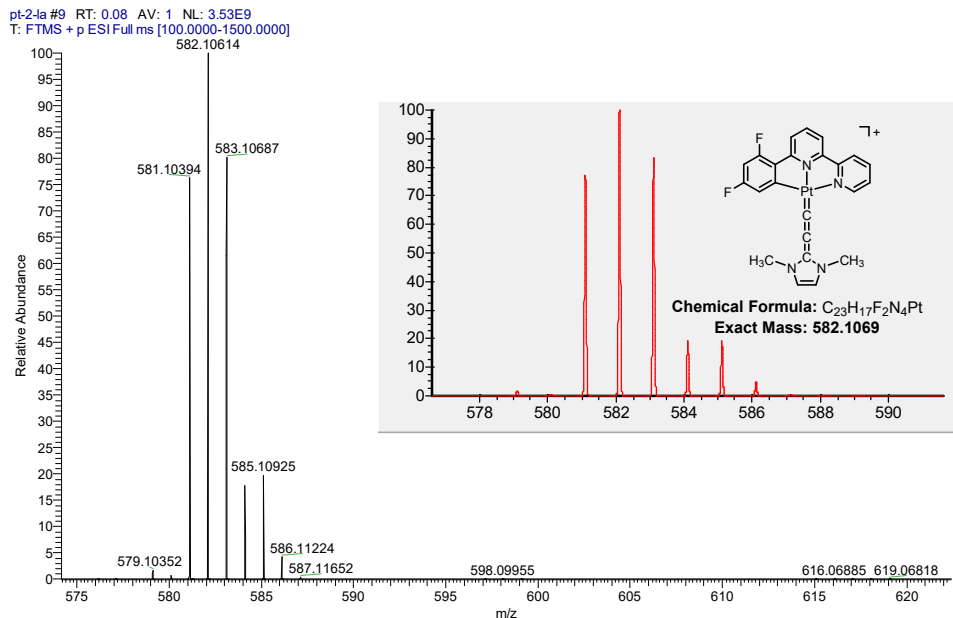


Negative mode:

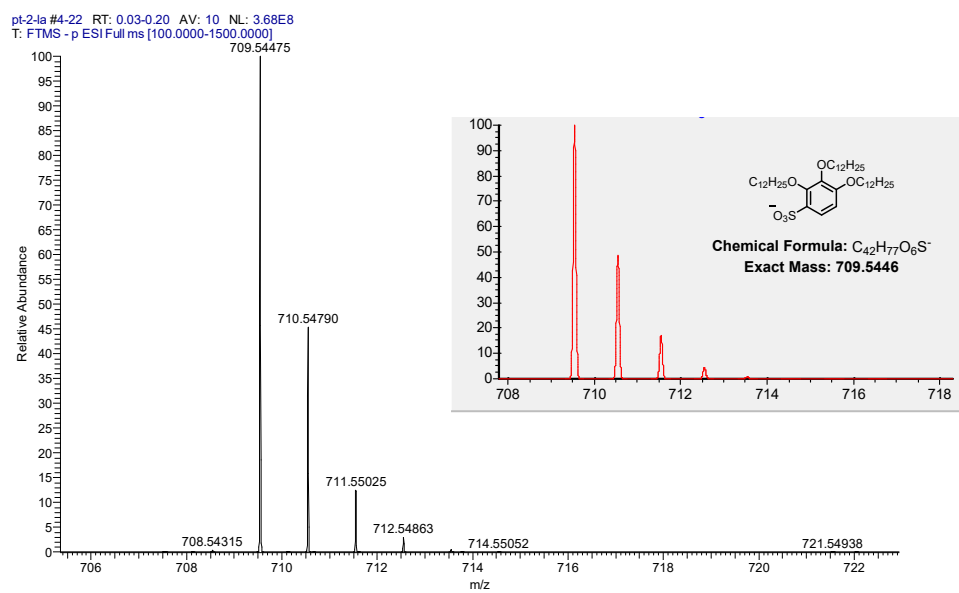


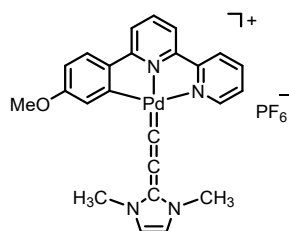


Positive mode:

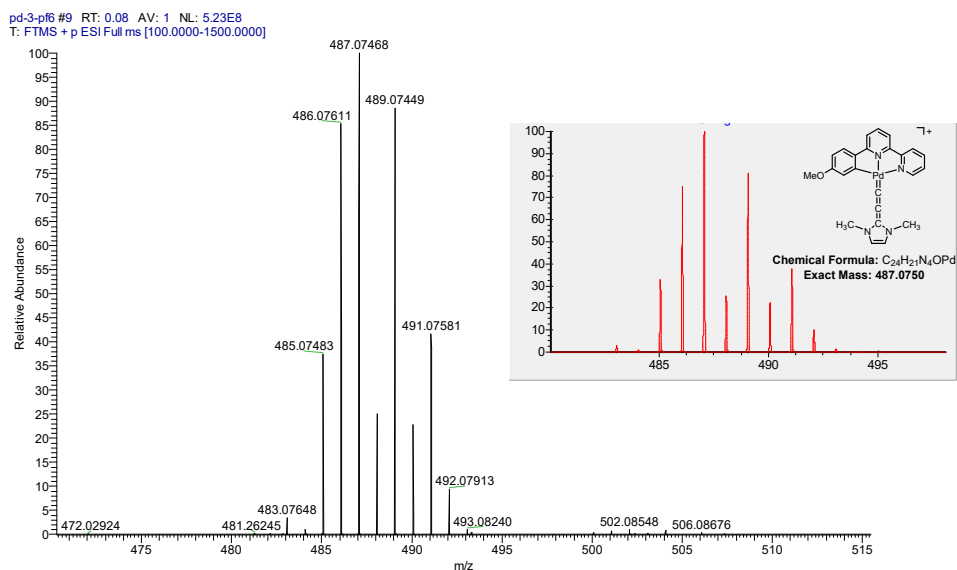


Negative mode:

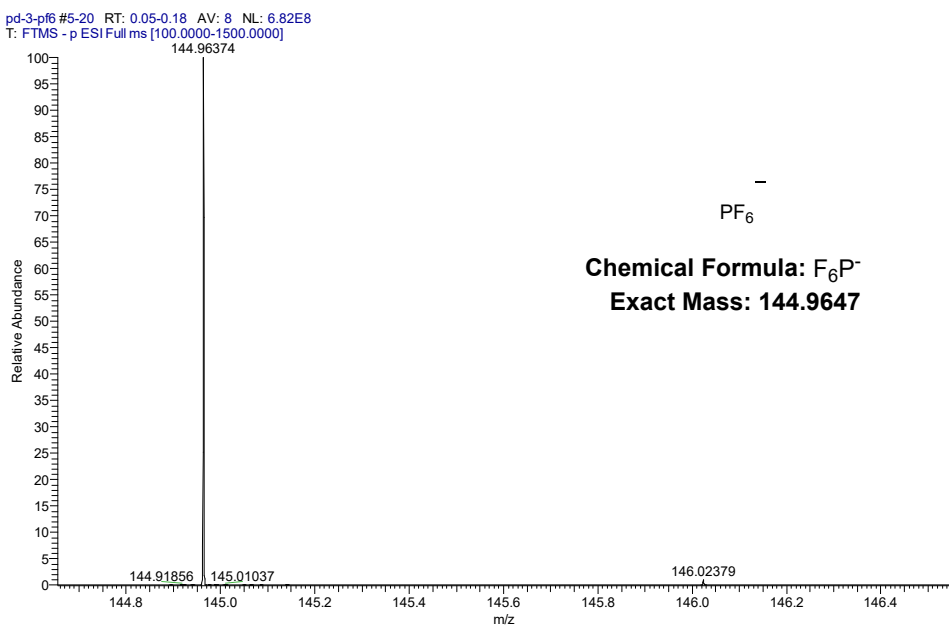


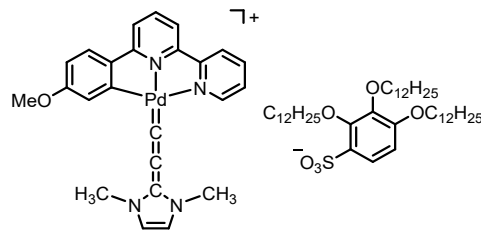


Positive mode:

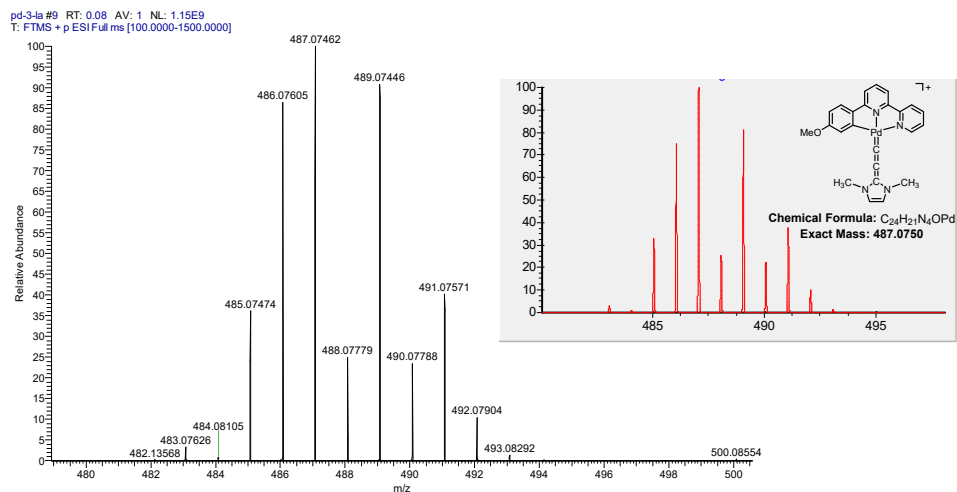


Negative mode:

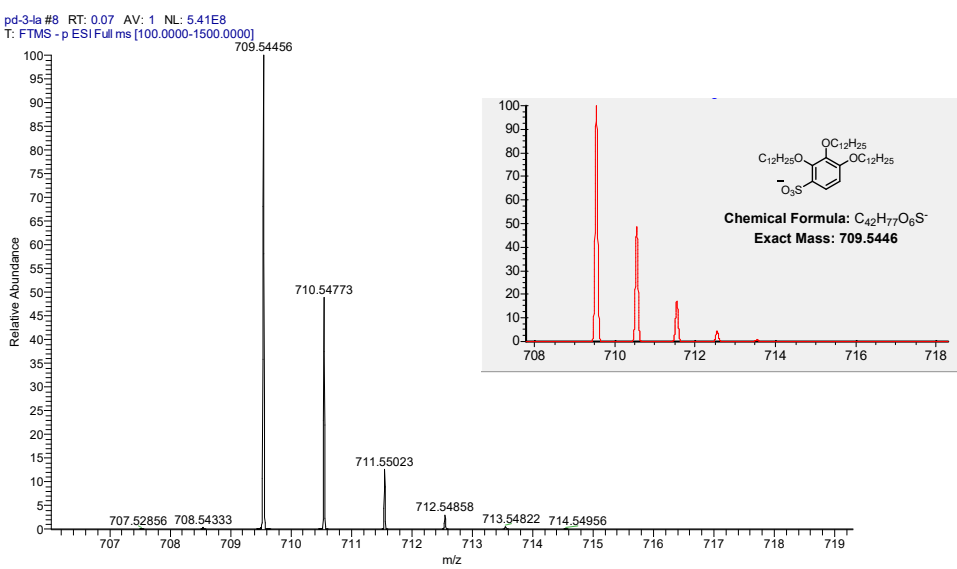


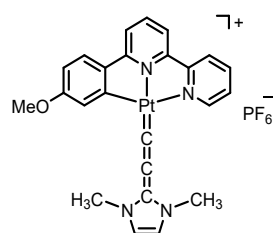


Positive mode:

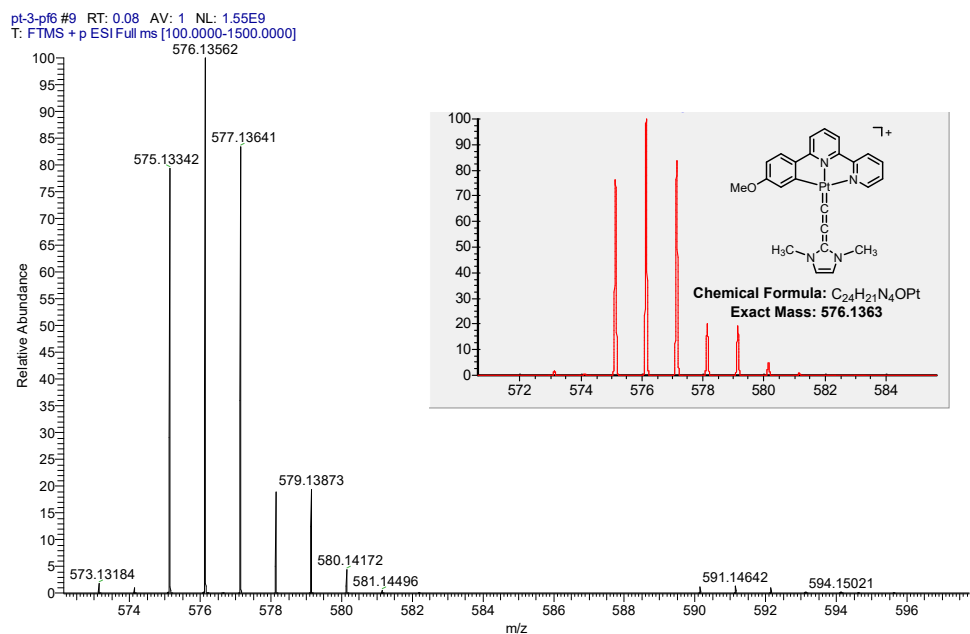


Negative mode:

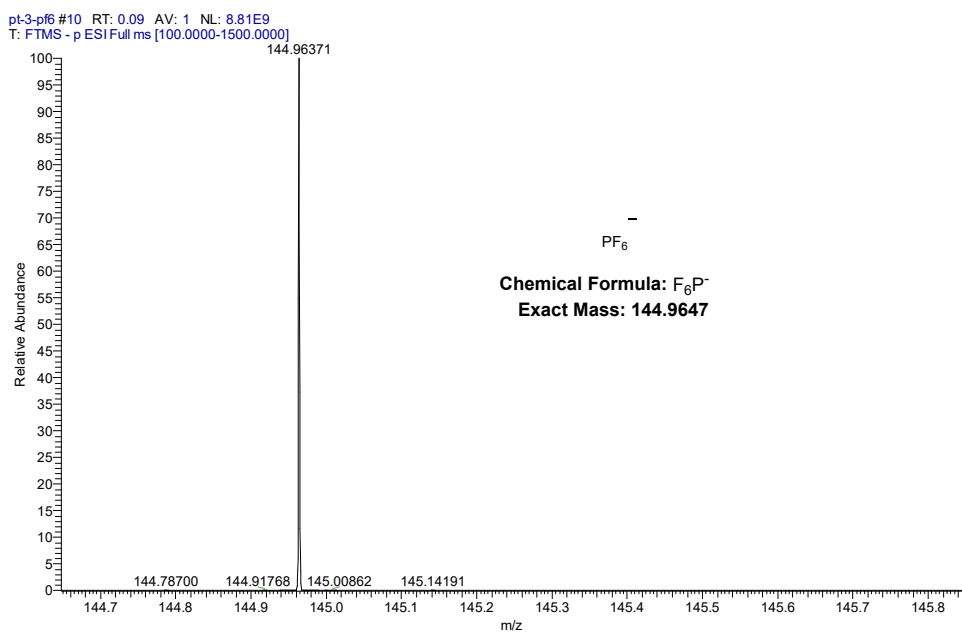


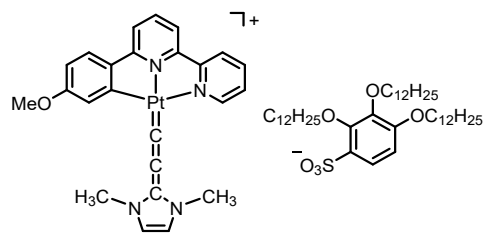


Positive mode:

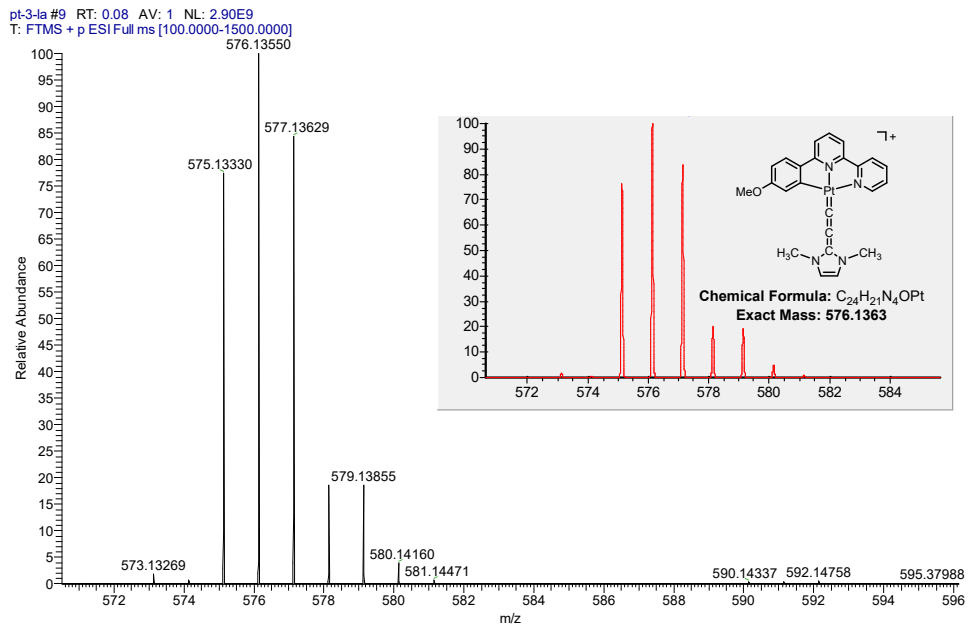


Negative mode:

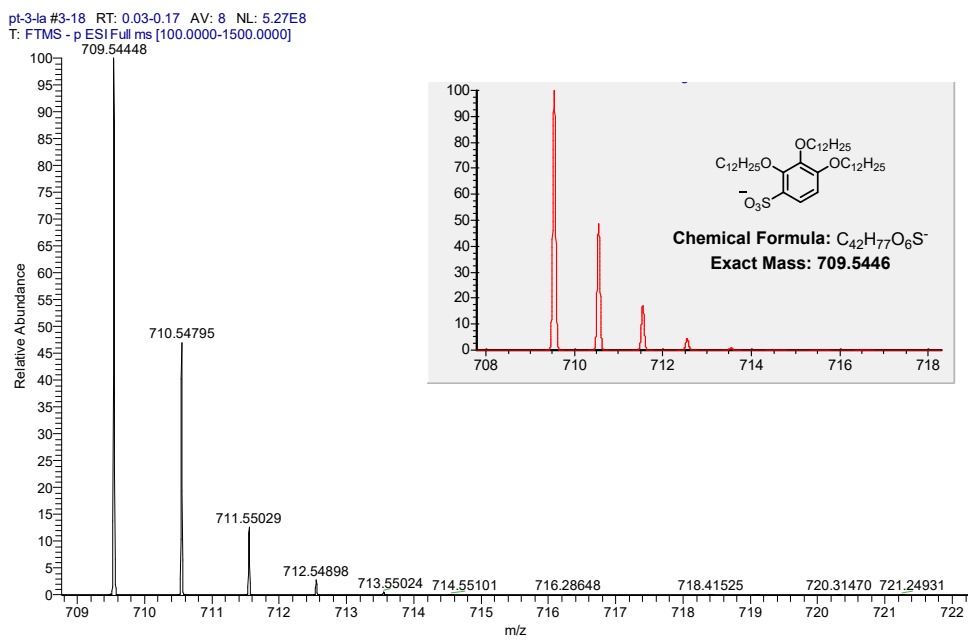




Positive mode:



Negative mode:



References:

1. Lu, W.; Mi, B.-X.; Chan, M. C. W.; Hui, Z.; Che, C.-M.; Zhu, N.; Lee, S.-T., *Journal of the American Chemical Society* **2004**, *126* (15), 4958-4971.
2. Stoccoro, S.; Soro, B.; Minghetti, G.; Zucca, A.; Cinelli, M. A., *Journal of Organometallic Chemistry* **2003**, *679* (1), 1-9.
3. Lin, J.; Zou, C.; Zhang, X.; Gao, Q.; Suo, S.; Zhuo, Q.; Chang, X.; Xie, M.; Lu, W., *Dalton Transactions* **2019**, *48* (28), 10417-10421.
4. Asay, M.; Donnadieu, B.; Schoeller, W. W.; Bertrand, G., *Angewandte Chemie International Edition* **2009**, *48* (26), 4796-4799.
5. Beginn, U.; Yan, L.; Chvalun, S. N.; Shcherbina, M. A.; Bakirov, A.; Möller, M., *Liquid Crystals* **2008**, *35* (9), 1073-1093.
6. Zhang, H.; Li, L.; Möller, M.; Zhu, X.; Rueda, J. J. H.; Rosenthal, M.; Ivanov, D. A., *Advanced Materials* **2013**, *25* (26), 3543-3548.
7. Zou, C.; Lin, J.; Suo, S.; Xie, M.; Chang, X.; Lu, W., *Chemical Communications* **2018**, *54* (42), 5319-5322.
8. De Greef, T. F. A.; Smulders, M. M. J.; Wolffs, M.; Schenning, A. P. H. J.; Sijbesma, R. P.; Meijer, E. W., *Chemical Reviews*, **2009**, *109* (11), 5687-5754.
9. Smulders, M. M.; Nieuwenhuizen, M. M. L.; De Greef, T. F. A.; Van der Schoot, P.; Schenning, A. P. H. J.; Meijer, E. W., *Chemistry-A European Journal*, **2010**, *16* (1), 362-367.
10. Ten Eikelder, H. M. M.; Markwoort, A. J.; De Greef, T. F. A.; Hilbers, P. A. J., *The Journal of Physical Chemistry B*, **2012**, *116* (17), 5291-5301.
11. Maarkvort, A. J.; Ten Eikelder, H. M. M.; Hilbers, P. J. J.; De Greef, T. F. A.; Meijer, E. W., *Nature Communications*, **2011**, *2*, 509-517.
12. Mayoral, M. J.; Rest, C.; Stepanenko, V.; Schellheimer, J.; Albuquerque, R. Q.; Fernandez, G., *Journal of the American Chemical Society*, **2013**, *135* (6), 2148-2151.